Author Manuscript

Author Manuscript

Author Manuscript

Author Manuscript

HHS Public Access

Author manuscript

Ultrasound Med Biol. Author manuscript; available in PMC 2020 May 01.

Published in final edited form as:

Ultrasound Med Biol. 2019 May ; 45(5): 1056–1080. doi:10.1016/j.ultrasmedbio.2018.10.035.

For whom the bubble grows: Physical principles of bubble nucleation and dynamics in histotripsy ultrasound therapy

Kenneth B. Bader[1], **Eli Vlaisavljevich**[2], and **Adam D. Maxwell**[3]

[1] - Department of Radiology and Committee on Medical Physics, University of Chicago, Chicago, IL

[2] - Department of Biomedical Engineering and Mechanics, Virginia Tech University, Blacksburg, VA

[3] - Department of Urology, University of Washington School of Medicine, Seattle, WA

Abstract

Histotripsy is a focused ultrasound therapy for noninvasive tissue ablation. Unlike thermally ablative forms of therapeutic ultrasound, histotripsy relies on the mechanical action of bubble clouds for tissue destruction. While acoustic bubble activity is often characterized as chaotic, the short-duration histotripsy pulses produce a unique and consistent type of cavitation for tissue destruction. In this review, the action of histotripsy-induced bubbles is discussed. Sources of bubble nuclei are reviewed, and bubble activity over the course of single and multiple pulses are outlined. Recent innovations in terms of novel acoustic excitations, exogenous nuclei for targeted ablation and histotripsy-enhanced drug delivery, and image-guidance metrics are discussed. Finally, gaps in knowledge of the histotripsy process are highlighted, along with suggested means to expedite widespread clinical utilization of histotripsy.

Keywords

Histotripsy; Focused Ultrasound; Cavitation; Ablation; Bubbles

Introduction

One of the primary goals of new medical technologies is the reduction of morbidity and complications in the course of treating a disease (Harrell and Heniford 2005; Jaffray 2005). Surgery is not well tolerated in elderly or comorbid patients (Turrentine et al. 2006). The development of new surgical techniques or instrumentation focuses on reducing procedural

Corresponding Author: Kenneth B. Bader, University of Chicago, Department of Radiology and Committee on Medical Physics, 5841 S. Maryland Avenue, MC 2026, Room 301B, Chicago, IL USA 60637, Phone: 773.702.8954 baderk@uchicago.edu.

Publisher's Disclaimer: This is a PDF file of an unedited manuscript that has been accepted for publication. As a service to our customers we are providing this early version of the manuscript. The manuscript will undergo copyediting, typesetting, and review of the resulting proof before it is published in its final citable form. Please note that during the production process errors may be discovered which could affect the content, and all legal disclaimers that apply to the journal pertain.

Disclosures of conflicts of interest

E. Vlaisavljevich is a consultant for HistoSonics (Ann Arbor, MI). A. Maxwell is a consultant and has financial interests with SonoMotion, Inc (South San Francisco, CA).

Author Manuscript Author Manuscript Author Manuscript Author Manuscript

complications, incisions, scarring, and recovery time (Jaffray 2005; Tejwani et al. 2017). Minimally invasive techniques such as laparoscopy and endoscopy achieve these goals, and are now standard procedure over open surgeries for many indications.

One of the most common minimally-invasive procedures is ablation. The clinical endpoint of ablation is to render the target tissue biologically nonviable. Minimally-invasive ablation can be achieved by several modalities, including radiofrequency alternating currents (Ni et al. 2005), microwaves (Lubner et al. 2010), laser energy (Gilling 2007; Oto et al. 2013), or freezing (Tatli et al. 2009). Proton beam therapy (Levin et al. 2005), x-ray or gamma radiation (Lindquist 1995), and focused ultrasound (Haar and Coussios 2007) are noninvasive options for ablation. Thermal ablation by high-intensity focused ultrasound (HIFU) is a promising technology for precise reduction of tumors or benign growths (Chaussy and Thuroff 2014; Kennedy et al. 2004; Xu et al. 2004). While the ablative efficacy of thermal HIFU has been demonstrated for select pathologies, it is limited by long treatment times (Lu et al. 2003) and requires MRI thermometry or quantitative B-mode imaging (Tavakkoli and Sanghvi 2011) for real-time feedback of treatment. Furthermore, thermal ablation of highly perfused tissue can be imprecise, inconsistent, or ineffective (Curley 2001).

An alternative to thermal ablation is mechanical disruption of tissue, such as thrombectomy (Stahr et al. 1999) or transurethral prostatectomy (Mebust et al. 1989). Histotripsy is a form of therapeutic ultrasound that produces mechanical disintegration of tissues that can be utilized to complement current ablative techniques, or as a stand-alone modality (Parsons et al. 2006; Roberts et al. 2006; Xu et al. 2004). The delivery of high-amplitude, short-duration histotripsy pulses repeatedly strains tissue at the subcellular level (Parsons et al. 2006; Roberts et al. 2006; Vlaisavljevich et al. 2016d). By applying a sufficient number of pulses, a target tissue structure can be homogenized precisely within the focal region. Within the treatment zone, cells are disintegrated into their subcellular constituents and the extracellular matrix is fragmented. Tissue outside the focal region remains intact (Fig. 1). Unlike thermal HIFU, the efficacy of histotripsy is not suppressed in highly vascularized tissue. Furthermore, both therapy delivery and the resulting tissue disruption can both be monitored in real time with either ultrasound or magnetic resonance imaging (MRI). The application of histotripsy to treat pathological tissue is predominately in the pre-clinical phase. However, histotripsy has the potential to be utilized in disease pathologies that would otherwise require surgical intervention (Bader et al.; Hall et al. 2007b; Hempel et al. 2011; Khokhlova et al. 2014; Kim et al. 2013; Kim et al. 2014a; Maxwell et al. 2011a; Owens et al. 2010; Schade et al. 2015; Styn et al. 2010; Vlaisavljevich et al. 2016c; Vlaisavljevich et al. 2013b; Xu et al. 2011; Zhang et al. 2017). Preclinical studies have investigated histotripsy for the treatment of thrombus obstruction (Bader et al. 2016b; Maxwell et al. 2011a; Sukovich et al. 2017; Zhang et al. 2017), fetal septal defects (Xu et al. 2010), kidney stones (Duryea et al. 2014), hepatocellular carcinoma (Khokhlova et al. 2014; Vlaisavljevich et al. 2013c; Vlaisavljevich et al. 2017b), renal carcinoma (Roberts et al. 2006), transcranial ablation (Sukovich et al. 2016), and biofilms (Bigelow et al. 2018), amongst others (Khokhlova et al. 2015). Furthermore, a clinical trial was recently completed whose primary outcome was to assess the safety of histotripsy technology to treat benign prostatic hyperplasia (Schuster et al. 2018).

Author Manuscript Author Manuscript Author Manuscript Author Manuscript

Tissue ablation is not resultant from the ultrasound pulse directly, but via the formation of acoustic cavitation or boiling bubbles. Cavitation has been detected previously with therapeutic and diagnostic devices in *in vitro* (Atchley et al. 1988; Fowlkes and Crum 1988; Roy et al. 1990) and *in vivo* (Haar and Daniels 1981; Harr et al. 1986; Holland et al. 1996; Hynynen 1991; Sapozhnikov et al. 2001) studies. Bubble activity can enhance the therapeutic efficacy for several different clinical applications (Bader et al. 2015a; Coussios and Roy 2008). However, inciting the intended bubble activity is difficult due to the episodic nature of cavitation (Coleman et al. 1996; Haworth et al. 2015; Holt and Roy 2001; Jensen et al. 2012; Sapozhnikov et al. 2001; Zhong et al. 1997). The stochastic behavior of cavitation can be attributed to the fact that separate aspects of bubble behavior (*e.g.* nonlinear oscillations, jetting, inertial collapse, etc.) are dictated by separate acoustic pressure thresholds (Apfel 1981; Bader and Holland 2012; Church 1988). That is, for the same set of initial cavitation nuclei, different types of bubble behavior can be generated depending on the insonation conditions. Histotripsy overcomes the stochastic nature of cavitation by operating with sufficient tension to *always* induce massive expansion of bubble nuclei, thereby instigating only a very specific and predictable type of bubble activity.

Three focused ultrasound insonation schemes are utilized in histotripsy to produce repeatable bubble activity (Fig. 2), summarized below:

- **Intrinsic-Threshold Histotripsy** delivers pulses with a single tensile phase (0.33-10 μs duration) sufficient to cause a cluster of bubble nuclei intrinsic to the target medium to undergo inertial cavitation.
- **Shock-Scattering Histotripsy** applies pulses 3-20 cycles in duration. The amplitude of the tensile phases is sufficient to cause individual nuclei to undergo inertial cavitation within the focal zone over the duration of the pulse. These bubbles scatter the incident shock waves geometrically, causing a dense bubble cloud to form in regions of constructive interference between the incident and scattered wave that exceed the threshold for intrinsic nucleation.
- **Boiling Histotripsy** employs pulses roughly 1-20 ms in duration. Absorption of the shocked pulse rapidly heats the medium, thereby reducing the threshold for intrinsic nuclei. Once this intrinsic threshold coincides with the peak negative pressure of the incident pulse, boiling bubbles form in the focus.

One of the key goals of this article is to explain how the different modes of histotripsy can be described in the context of a bubble population or threshold that appears to be intrinsic to a given medium. This review discusses theoretical and experimental aspects of histotripsy-generated cavitation and boiling, including pathways to reliably achieve dense bubble clusters necessary for tissue disintegration. The topics of bubble nucleation, cavitation, and boiling by ultrasound have a vast history and body of literature. Discussion is necessarily limited to descriptions of those areas that achieve the specific effects described in histotripsy. Whenever possible, discussion is tied to relevant historical precursors and literature that forms a foundation for the observations of bubbles in histotripsy. To gauge bubble activity, Apfel (1981b) formulated three golden rules: 1) Know thy sound field, 2) Know thy liquid,

Author Manuscript Author Manuscript Author Manuscript Author Manuscript

and 3) Know when something happens. Our understanding of histotripsy-induced bubble activity will be viewed through this framework.

Know thy sound field

While ultrasound is known most ubiquitously as a diagnostic imaging modality, its therapeutic use dates back a century. Early studies on ultrasound-induced bioeffects were conducted after World War I, predominately continuing war-time observations of sonar-induced fish death (Langevin 1920; Harvey and Loomis 1928) or noninvasive heating (Freundlich et al. 1932). Therapeutic ultrasound came into earnest with William and Frank Fry at the University of Illinois (O' Brien and Dunn 2015). Their preliminary *in vivo* studies with focused sources (Fry et al. 1950; Fry 1952; Fry et al. 1970) culminated in the treatment of 88 Parkinson's disease patients (Fry and Fry 1960), and cemented the use of ultrasound as a therapeutic modality.

Linear propagation in focused ultrasound

The diffraction field of a focused source provides a high intensity within the target volume, but low intensity in the intervening tissues. Ultrasound is commonly generated in histotripsy by piezoelectric transducers operating at frequencies near 1 MHz, with focusing produced by acoustic lenses or curvature of the piezoelectric material itself (Kim et al. 2014b). Spherically focused sources produce a focal region of high pressure amplitude, where the ratio of amplitudes between the focal peak and transducer surface is defined by the focal gain, G. For most histotripsy applications, large aperture transducers with short focal distances are used to ensure G is greater than ~ 30 (Hall et al. 2009; Maxwell et al. 2009; Maxwell et al. 2017; Xu et al. 2004). The focus forms as a prolate ellipsoidal volume, with typical −6 dB dimensions of ~10 mm along the acoustic axis and 1-2 mm width lateral to the acoustic axis in a linear (low-amplitude) regime (Rosnitskiy et al. 2017).

Nonlinear propagation in focused ultrasound

In addition to the effects of linear propagation and focusing, the high intensity output of a therapeutic source will induce nonlinear distortion of the pressure waveform (Hallaj and Cleveland 1999). Distortion of the sinusoidal pressure waveform is due to a local variation in the pressure-dependent sound speed, $c(p_a)$, which can be expressed to first order as (Hamilton and Blackstock 1998):

$$c(p_a) = c_0 + \frac{\beta p_a(t)}{\rho_0 c_0} \quad (1)$$

where β is the coefficient of nonlinearity of the medium, c_0 is the ambient medium sound speed, ρ_0 is the ambient medium density, and p_a is the acoustic pressure at time t. The transition of energy from the fundamental frequency into higher harmonics results in a steepening of the waveform (see Fig 3). With sufficient amplitude and propagation distance, any pressure pulse will be distorted into a saw-tooth waveform (Pierce 1989). For a focused source, the combined effects of diffraction and nonlinearity cause waveform distortion that

Author Manuscript Author Manuscript Author Manuscript Author Manuscript

lead to a shock wave (Fig. 3). The resultant pressure waveform in the focus is asymmetric, with a larger amplitude and shorter duration positive pressure in comparison to the negative pressure (Bessonova et al. 2009). Shock waves can be generated for all forms of histotripsy therapy, and are essential to generate the bubble activity necessary for ablation in shock-scattering and boiling histotripsy.

The degree of nonlinear distortion in the pressure waveforms additionally depends on the transducer geometry and frequency. The most efficient means of generating large tension within the focus are sources with high focal gain or low *f*-number, defined for a spherically focused source as the ratio of focal distance to aperture diameter. As nonlinear effects accumulate with propagation distance (Hamilton and Blackstock 1998), the pressure within the focus of low *f*-number sources (~ 0.5–0.7) consequently remains in a near-linear regime when generating cavitation (Vlaisavljevich et al. 2017a). As the *f*-number of the source increases, a nonlinear wave will form as depicted in Fig. 3. Sources with *f*-numbers between 0.7 and 1 still have sufficient focal gain to promote cavitation activity via shocked excitations with fundamental frequencies generally less than 1.5 MHz. If the transducer is further unfocused (*f*-number greater than 1), robust shock waves are formed at relatively low pressure amplitudes. The pressure waveform can reach a condition of acoustic saturation with a characteristic sawtooth waveform. At the acoustic saturation limit, the focal pressure does not increase with higher transducer output as the additional energy is dissipated in the shocks. Acoustic saturation occurs at pressures where bubble nucleation is stochastic for transducers with higher *f*-numbers.

Know thy liquid

The second of Apfel's golden rules denotes knowledge of cavitation nuclei within the medium. In this section, an overview of classical and heterogeneous nucleation theory in water will be presented. This will be followed by a discussion of potential nuclei found *in vivo*, and a description of the influence of histotripsy insonation parameters on the cavitation threshold. A summary of the threshold for histotripsy-induced cavitation will also be reported.

Bubble nucleation in water

Water mimics many acoustic properties of soft tissues. For this reason, the study of bubble formation in water has been an important focus in understanding histotripsy-induced cavitation. Flynn (1964) considered bubble nucleation to be a form of boiling, transitioning a liquid-based medium to a vaporous or gaseous state. The likelihood of bubble nucleation depends strongly on the quality of the water. In the case of pure liquids without exogenous nuclei, bubbles must be created through a first-order phase transition as described by classical nucleation theory (CNT). The relationship for the energy of a bubble to form W is the sum of the energy to displace the surrounding liquid volume, the generation of vapor, and the energy to create the bubble surface (Church 2002; Fisher 1948):

$$W = 4\pi R^2\sigma + \frac{4}{3}\pi R^3(p_0 + p_a - p_v) \quad (2)$$

Author Manuscript Author Manuscript Author Manuscript Author Manuscript

where R is the radius of the cavitation nucleus, σ is the medium surface tension, p_0 is the ambient pressure, and p_v is the vapor pressure. Thermal fluctuations are the most ubiquitous source of energy in fluids. According to CNT, these fluctuations will produce bubbles of 1 Å diameter spontaneously. The lifetime of these spontaneous nuclei is estimated to be ~ 10^{-18} s as the Laplace pressure, given by $2\sigma/R$, causes the bubble to dissolve and the vapor to recondense within the fluid (Yang and Prosperetti 2008).

The nucleation rate described by CNT is dictated by Maxwell-Boltzmann statistics (Church 2002). Thus, a pure liquid whose only source of nuclei is thermal fluctuations has no tension level at which there is a 100% certainty in cavitation. To allow direct comparison to the discussion in this manuscript and other studies (Arvengas et al. 2011b; Herbert et al. 2006; Maxwell et al. 2013; Vlaisavljevich et al. 2015b), we define the cavitation threshold as peak negative pressure for which the probability of nucleating one or more bubbles during a pulse exceeds 50%. For histotripsy, this definition of the cavitation threshold is a useful measure because it defines the pressure at which cavitation becomes likely to occur each pulse. The probability of producing cavitation can be altered by multiple factors. Applying tension over a larger volume of fluid or over a longer duration will result in an increased likelihood of cavitation (Church 2002). Similarly, heating or cooling the medium will alter the cavitation threshold, as indicated by the temperature-dependent vapor pressure and surface tension in Eq. (2).

Efforts have been made to characterize the tensile strength of water (Briggs 1950; Couzens and Trevena 2002; Herbert et al. 2006; Zheng et al. 1991). One challenge in such a measurement is achieving water purity, as exogenous nuclei are not described by CNT. Measurement of the threshold tension in water predicted by CNT, 140 MPa, has only been achieved in quartz inclusions samples (Zheng et al. 1991) or within very short time frames (Stan et al. 2016). Efforts to replicate similar tensile values in water have yet to be achieved with other experimental designs. Picosecond X-ray (Stan et al. 2016) or nanosecond laser (Li et al. 2015) sources have generated cavitation at tensions of 100 and 60 MPa, respectively. Acoustic methods apply tension time scales on the order of 0.1 μs to seconds, and an upper limit of 30 MPa tension has been measured prior to cavitation (Bader et al. 2012b; Briggs 1950; Herbert et al. 2006; Maxwell et al. 2013; Vlaisavljevich et al. 2015b) (Fig. 4). Beyond 30 MPa tension, the probability of cavitation occurring is very close to 100% for such acoustic sources. The discrepancy between pico- and microsecond nucleation thresholds may have several contributing factors. Chemical relaxation phenomenon may cause changes in water properties at different time scales (Pierce 1989). The formulation of bubble surface tension in bulk fluids are not well characterized at the molecular level, requiring simulations to refine the understanding of gas/water interfaces (Bruot and Caupin 2016; Bykov and Zeng 2001). Another possibility is the presence of liquid impurities that generate nuclei larger than the spontaneous nuclei associated with thermal fluctuations (Crum 1979; Fowlkes and Crum 1988; Harvey et al. 1944).

Sources of cavitation nuclei

In the event cavitation nuclei are present within the medium, the pressure necessary to cause explosive bubble growth can be predicted. The growth of an existing bubble nucleus in

Author Manuscript Author Manuscript Author Manuscript Author Manuscript

response to quasi-static changes in fluid tension can be described by the Blake threshold, p_l (Blake 1949):

$$p_l = p_0 - p_B = p_v - \frac{4\sigma}{3}\sqrt{\frac{2\sigma}{3\left(p_0 + \frac{2\sigma}{R_0} - p_v\right)}} \quad (3)$$

When the Blake threshold is exceeded (Fig. 5), the bubble will grow unbounded until the tension is removed or buoyancy causes the bubble to escape the liquid space. While an acoustic wave is a dynamic pressure fluctuation, the measured threshold for histotripsy excitations (~ 30 MPa) correspond to nuclei on the order of a few nanometers in diameter (Fig. 5). The resonant angular frequency of the nucleus ω_0 can be written in terms of the medium properties (Yang and Church 2005):

$$\omega_0 = \sqrt{\left\{3\kappa\left(p_0 + \frac{2\sigma}{R_0} - p_v\right) - \frac{2\sigma}{R_0} + p_v - \frac{4\mu^2}{\rho R_0^2} + 4G\right\}/(\rho R_0^2)} \quad (4)$$

where G is the medium linear shear modulus, μ is the dynamic viscosity, κ is the ratio of specific heats, and R_0 is the radius of the cavitation nucleus. The natural period of oscillation for a nanometer-sized nucleus is approximately $\frac{1}{2\pi\omega_0} \sim 50$ ps (Fig. 5), much shorter than the tensile period of the histotripsy source. Thus the tensile period during therapeutic insonation "feels" like a quasi-static change in pressure to the small nuclei.

There are many potential nanoscale nuclei sources. Cosmic rays carry sufficient energy to overcome the bubble nucleation threshold, but are too infrequent to impact the histotripsy cavitation process (244 events/sec/m^3 in water) (Greenspan and Tschiegg 1967). Harvey et al. (1944) proposed that bubble stabilization can be achieved in the crevices of solid motes. The air/water interface curvature bows into the mote, causing the corresponding Laplace pressure to oppose gas diffusion out of the stabilized nucleus (Apfel 1970a; Crum 1979). While observing microscopic impurities in agarose gels, Yount (1979) surmised that a permeable skin coating around the nucleus reduces surface tension and prevents outward diffusion of gas. Nuclei stabilization has been proposed through ionic charges surrounding gas molecules, entities described as charged bubbles or 'bubstons' (Bunkin et al. 1996; Sankin et al. 2006). These mechanisms allow indefinite existence of bubble nuclei, but require that the water contain impurities – an almost unavoidable occurrence (Bader et al. 2012b; Flynn 1964). Thus, careful preparation of the water and vessel is required to minimize nuclei that can be expanded by low amplitude pulses.

There is evidence that bubble nuclei exist *in vivo*. These nuclei can be *extrinsic* or *intrinsic*. Here, we classify *intrinsic* nuclei as the seeds for a bubble that permeate a medium, and would be found in any physiologic conditions. *Extrinsic* nuclei require an inhomogeneity to activate cavitation. While found only in discrete locations, the existence of extrinsic nuclei is not precluded *in vivo*. The oldest evidence for extrinsic bubble nuclei comes from naval

Author Manuscript Author Manuscript Author Manuscript Author Manuscript

observations of divers have suffering from decompression sickness (Behnke 1945). Bubble activity has been observed in supersaturated *ex vivo* tissue, akin to conditions occurring during the ascension of divers (Crum et al. 2005). Gas-containing organs, such as intestines and lungs, are considered the most susceptible to hemorrhagic injury by ultrasound exposure (Carstensen et al. 2000; Holland et al. 1996). Bubbles have been detected via diagnostic ultrasound on kidney stones within the urine (Bailey et al. 2005; Leighton et al. 2008). Cavitation has also been produced in urine and surrounding tissues during shock wave lithotripsy, albeit at significantly higher pressure amplitudes than the thresholds reported for lungs/intestinal injury (Dalecki et al. 1997; Miller and Gies 2000). The urine contains solid microcrystalline inclusions that may also serve to stabilize nuclei (Fogazzi 1996). Extrinsic nuclei are also activated during tissue heating, such as during thermal HIFU procedures (ter Haar and Daniels 1981; ter Harr et al. 1986). The sources of extrinsic cavitation nuclei triggered at diagnostic ultrasound levels are presumably harbored in crevices such as calcifications within kidney stones, arterial plaque, or gas bodies (Kim et al. 2010; Simon et al. 2018). Thus, we see that extrinsic nuclei do not exist without some form of gas-body activation or gas-harboring entity (Miller 2007).

In contrast, intrinsic nuclei are ubiquitous to the medium. Histotripsy-induced cavitation *in vivo* occurs at peak negative pressures between 10 to more than 25 MPa, similar to pressures at which consistent nucleation is observed in water. Cavitation can be reliably produced at these pressure levels in water-based media, with a sharp decline in the nucleation rate at lower amplitudes. Peak negative pressure thresholds of 26.2 to 29.4 MPa for 1-MHz pulses of 2-cycle duration were observed for water, 5% and 15% gelatin hydrogel tissue phantoms, and *ex vivo* canine blood, liver, and kidney (Fig. 4). Cavitation was not detected at pressure amplitudes less than 13.5 MPa for any of these water-based media. For media that are not predominately water-based (canine adipose tissue, 1-3 butanediol, and olive oil), the cavitation thresholds does not fall within the 26.2 to 29.4 MPa range (15.4, 35.2, and greater than 36 MPa, respectively).

The tight grouping of the intrinsic threshold for water-based medium point to an extremely robust and predictable subset of bubble nuclei that are activated by short duration pulses, requiring peak negative pressures in excess of 10 MPa to initiate cavitation. Experiments have demonstrated the ubiquity of this population of bubble nuclei in water, although attempts to isolate and remove these nuclei from water have not been successful (Herbert et al. 2006). Histotripsy exploits this population of nuclei to repeatably form cavitation clouds in tissues repeatedly. The close agreement between the intrinsic cavitation threshold of water-based soft tissues with the intrinsic threshold of water suggests these nuclei are contained within the water component of the tissue. A recent study of histotripsy at the cellular level noted cavitation bubbles were only observed to form in the extracellular space, which has a much larger volume of liquid water compared to the intracellular environment (Vlaisavljevich et al. 2016d). However, further work is needed to ascertain the nature of these nuclei and the precise location of nucleation in tissues.

Author Manuscript Author Manuscript Author Manuscript Author Manuscript

Dependence of intrinsic threshold on histotripsy insonation parameters

The frequency of single-cycle pulses appears to have minimal influence on the intrinsic cavitation threshold, which increases by less than 3 MPa from 0.345 to 3 MHz in agar phantoms (Vlaisavljevich et al. 2015b). Significant decreases in the cavitation threshold were observed at low frequency insonations (345-500 kHz) in 90% gas saturated water, likely due to sources of extrinsic nuclei. The total focal volume, and therefore the total number of insonated nuclei, will be dictated by the frequency and transducer geometry. No significant changes have been observed in the intrinsic cavitation threshold for 500-kHz transducers with *f*-numbers between 0.5 and 0.9 (Vlaisavljevich et al. 2017a).

The histotripsy pulse duration determines the total time the volume is subject to tension, and is also a determining factor in the nucleation of cavitation. *In vitro* and *ex vivo* studies with multiple cycle histotripsy pulses have demonstrated shock-scattering bubble clouds can be generated at lower amplitude compared to single cycle tensile pulses (10-25 MPa vs. 26-29 MPa) (Maxwell et al. 2011b; Vlaisavljevich et al. 2014). It is clear that the probability of cavitation increases with longer-duration pulses (Haller et al. 2018), although a general quantitative dependency based on the insonation parameters (e.g. fundamental frequency, degree of nonlinearity, focal volume, etc.) has yet to be established. Li *et al.* have measured thresholds for 1-ms pulses in various media (2014b). The probability reached near 50% for peak negative pressures of 12.5 MPa in pure water, and even lower in *ex vivo* tissues. Haller et al. (2018) found an increase in the cavitation threshold from 1.1 MPa to 4.6 MPa as the duration of a 1.06-MHz pulse decreased from 1 s to 25 cycles in a 3% agar phantom. More research is needed to reach a general understanding of how these thresholds vary with parameters and measurement systems.

Dependence of intrinsic threshold on medium parameters

Systematic studies have ascertained the dependence of cavitation probability as a function of medium stiffness (Young's modulus) for single-cycle excitations *in vitro* (Vlaisavljevich et al. 2015b). No correlation was found between the intrinsic threshold and the stiffness of agar phantoms for Young's moduli from 0 to 930 kPa. For *ex vivo* samples, the intrinsic threshold increased 2 MPa for liver (Young's modulus 8.7 kPa) compared to tendon (Young's modulus 380 MPa).

In addition to stiffness, other medium properties may also play a role in the intrinsic threshold. Cavitation probabilities in excess of 50% have not been measured in more viscous liquids (1,3 butanediol and olive oil, $\mu = 97$ and 84 cP, respectively, versus 1 cP for water) (Arvengas et al. 2011b; Maxwell et al. 2013). The temperature dependence of the intrinsic threshold has been explored *in vitro* (Arvengas et al. 2011a; Vlaisavljevich et al. 2016e). A monotonic decrease in the intrinsic threshold from 29.8 to 14.9 MPa was observed as the temperature of the medium increased from 10°C to 90°C. The measured temperature-dependent cavitation threshold matches the relative changes with temperature predicted by a CNT model (Arvengas et al. 2011a; Vlaisavljevich et al. 2016e). The surface tension was adjusted to 27.5% of its classical value in the CNT model to match the measured threshold values. Similar reductions in the contributions of surface tension have been suggested for bubble formation during other ultrasound exposures (Herbert et al. 2006). Temperature

Author Manuscript Author Manuscript Author Manuscript Author Manuscript

increases also change the surface tension, vapor pressure, and viscosity to promote bubble nucleation favorably. It should be noted that simulations of histotripsy-induced bubble activity indicate little change in the maximum bubble diameter over the same range of medium properties corresponding to these temperatures (Bader and Holland 2016).

Know when something happens

Apfel's final golden rule, know when something happens, refers to detecting a cavitation event. The type of cavitation-induced event, and therefore the means by which cavitation is detected, is dictated by the cavitation dynamics. One criterion for the onset of inertial cavitation is violent bubble collapse, occurring once the bubble wall velocity approaches the sound speed in the medium (Datta et al. 2008; Gruber et al. 2014; Haworth et al. 2017). Prior to the inertial collapse, the overwhelming tension in the incident histotripsy pressure waveform forces bubble growth during insonation. While the expansion can be described to first order in terms of a Blake cavity, the overarching bubble dynamics depend on the form of histotripsy.

Intrinsic-threshold histotripsy

Intrinsic-threshold histotripsy relies on single-cycle pulses with sufficient tension to cause massive expansion of bubble nuclei in the medium. Single bubbles appear in the focus when the tension is near the intrinsic threshold (Maxwell et al. 2013). As the pressure amplitude is increased, the cavitating volume is increased in proportion to the volume of the focal zone exceeding the intrinsic threshold (Vlaisavljevich et al. 2017a). Once expansion ensues, the bubble dynamics match that of a pure Blake cavity during the acoustic excitation. The bubble grows over the duration of the pulse with sufficient momentum that expansion continues beyond the completion of the excitation (Vlaisavljevich et al. 2015c). Once growth is halted, and the bubble will collapse inertially under the ambient pressure.

For the incident waveform to exceed the intrinsic threshold, high-gain sources with *f*-numbers between 0.5 and 1 are utilized. The focal volume is smaller with a reduction in the *f*-number of the source, thereby refining the region over which bubble activity is generated. The smaller focal volume has the added effect of reducing the waveform nonlinearity for a given peak negative pressure (Rosnitskiy et al. 2017). That is, bubbles can be nucleated prior to the onset of strong nonlinearities for intrinsic threshold pulses. The bubble cloud density within the focal regions is also significantly increased for low *f*-number sources (Vlaisavljevich et al. 2017a).

While the maximum bubble size is generally proportional to the peak negative pressure, only modest increases in the bubble size are observed for tensions in excess of the intrinsic threshold (Fig. 6) (Vlaisavljevich et al. 2015c). The activation of intrinsic nuclei transfers energy from the acoustic wave into the potential and kinetic energy of the bubbles, thus limiting the negative pressure that contributes to the cavitation process (Pishchalnikov et al. 2005). Further increases in amplitude of the acoustic source will result in a greater number of activated nuclei within the focal zone, but bubbles may not experience tension in excess of the intrinsic threshold. A dense bubble cloud is typically nucleated for tensions at the intrinsic threshold (Vlaisavljevich et al. 2015c). The limitation of the maximum bubble size

Author Manuscript Author Manuscript Author Manuscript Author Manuscript

may also be reflective of the strong bubble-bubble interaction (Wang and Brennen 1999) or acoustic shielding of the incident pulse by bubbles proximal to the transducer (Commander and Prosperetti 1989).

Shock-scattering histotripsy

The *f*-number of transducers used for shock-scattering histotripsy are generally between 0.7 and 1.0 to compromise between focal gain necessary to activate intrinsic nuclei into extrinsic micrometer-sized scatters with the degree of nonlinearity to generate a shock wave (Vlaisavljevich et al. 2017a; Xu et al. 2006a). The resultant waveforms are highly nonlinear pulses 3-20 cycles in duration with peak negative pressures between 15 and 25 MPa. Micrometer-sized bubbles are formed within the focal region, though the compressional pressure of the shock wave mitigates the bubble growth rate compared to intrinsic threshold pulses (Maxwell et al. 2011b). In limiting cases where bubble nucleation has a low probability, hundreds or thousands of pulses may be applied before cavitation and the ensuing cloud are achieved. As the bubble grows over the duration of the pulse, a larger portion of the energy in the incident shock wave is backscattered toward the transducer. The bubble-tissue interface acts as a pressure-release boundary condition (Pierce 1989), and the scattered shock wave is inverted with respect to the incident pressure waveform (Fig. 7, left). Once the bubble is sufficiently large, the tension of the total wave field comprising the combined incident and backscattered waves will exceed the intrinsic threshold. The scattered wave nucleates numerous cavitation bubbles between the initial bubble and the histotripsy source. Additional bubbles are nucleated as the subsequent shock scatters from the bubble cloud formed during the previous cycle. The bubble cloud grows against the direction of the incident pulse until the insonation ends, or the extent of the bubble cloud reaches the edge of the focal zone (Fig. 7, right). In addition to acoustic sources, scattering bubbles can be alternatively generated via pulsed laser sources (Horiba et al. 2017).

Although the compressional component of the pulse can exceed 80 MPa, the bubbles that initiate the shock-scattering process tend to expand throughout the duration of the pulse (Maxwell et al. 2011b). The inertia of the large bubble (10-100 μm in diameter) is unable to respond to the short compressional phase of the histotripsy pulse (Ainslie and Leighton 2011). The lack of collapse during the compressional phase of the histotripsy pulse indicates a reversal in the time scales relative to the initial nucleus: the resonant frequency of the nucleus is much larger than the fundamental frequency of the incident histotripsy pulses (see Fig. 5). During expansion, the effective resonant frequency of the bubble lowers significantly compared to the high frequencies associated with the shock wave.

The strength of shock scattering is strongly dependent on the shape of the initial scatterer. The shocked, asymmetric excitation may deform the bubble from its spherical shape into a hemisphere or a concave form, as depicted in Fig. 7 (Maxwell et al. 2011b). Distortion of the bubble shape can occur due to the pressure differential across the bubble when the shock is incident on one side, and is related to jetting phenomena (Brujan et al. 2001). The distortion is consistent with numerical models of shock wave-induced bubble behavior (Johnsen and Colonius 2008). Scattered fields from hemispherical bubbles are cone shaped, and have the largest field strengths within $\lambda/2$ from the scattering interface (λ is the acoustic wavelength

Author Manuscript Author Manuscript Author Manuscript Author Manuscript

of the histotripsy pulse fundamental frequency) (Maxwell et al. 2010a). Consequently, new bubbles are nucleated in close proximity to the initial bubble. The peak negative pressure of a scattered field from a spherical bubble is significantly reduced compared to a hemispherical bubble (Maxwell et al. 2010a). Bubble clouds can still form, however, when the pulse scattered from a spherical bubble interferes constructively with the subsequent tensile phase of the shock-scattering histotripsy pulse.

The formation of each layer of bubbles serves as a new interface from which the shock wave scatters, causing the bubble cloud to grow. The axial growth rate is approximately λ/3 per acoustic cycle once shock scattering is initiated (Maxwell et al. 2011b). The closest pressure peak of constructive interference would occur at a distance λ/4 from the bubble surface for a linear waveform, and increase to λ/2 for a sawtooth waveform. Depending on the degree of waveform distortion and the region over which new bubbles occur during a cycle, the peak tension can occur anywhere between these values. The nonlinear field decreases quickly with distance beyond the focal zone (Rosnitskiy et al. 2017), and is the limiting factor for the axial extent of the bubble cloud. The lateral growth of the cloud (i.e. perpendicular to the central axis of the histotripsy source) is largely independent of the pulse duration and is limited to the extent of the beam width.

Boiling histotripsy

Thermal ablation with focused ultrasound denatures tissue over the course of seconds or minutes. The heating rate Q is proportional to the intensity of the sound field and attenuation in the focus (Hallaj and Cleveland 1999). Shock waves, consisting of a series of harmonics, dissipate energy much more rapidly over a distance compared to a linear waveform (Hamilton and Blackstock 1998). Under the condition that heating occurs quickly enough, the tissue can boil and cause mechanical disintegration prior to producing any noticeable thermal effects. Such is the case with boiling histotripsy.

Shock-induced heating during a boiling histotripsy pulse will alter the medium properties and increase the likelihood of bubble generation. The time for onset of boiling (t_b) can be estimated under the assumption that the heating rate is sufficiently large to neglect thermal diffusion (Canney et al. 2010):

$$t_b = \frac{\Delta T C_v}{Q} \quad (5)$$

where C_v is the heat capacity, and ΔT is the temperature difference required to reach a boiling temperature, 100°C. When a shock wave is fully formed, the heating rate can be estimated via weak shock theory as: $Q_S = \beta f_0 A_S^3 / 6 c_0^4 \rho^2$ (Canney et al. 2010), where A_s is the shock wave amplitude, and f_0 is the fundamental frequency of the insonation. A shocked waveform increases the heating rate significantly compared to a linear pressure waveforms of the same pressure amplitude, allowing boiling to occur within milliseconds. However, the onset of boiling requires bubble nucleation. Increases in temperature decrease the threshold tension required to achieve intrinsic nucleation, which reduces to ~ 15 MPa at 90 °C

Author Manuscript Author Manuscript Author Manuscript Author Manuscript

(Vlaisavljevich et al. 2016e). Rapid heating may result in local tissue temperatures beyond 100 °C, further reducing the threshold until a nucleus is generated. The stochastic processes associated with the activation of intrinsic nuclei in heated media may explain variability of the time-to-boil observed in experiments (Canney et al. 2010).

The parameter space over which boiling can be initiated within 10 ms (a reasonable time to avoid thermal effects to the tissue) is well defined in soft tissues, as depicted in Fig. 8A. With respect to the insonation parameters, the calculated time to boil is dependent on the fundamental frequency and shock amplitude. Given the complex relationship between the intrinsic nucleation and temperature (Vlaisavljevich et al. 2016e), a correlation between the time to boil and the peak negative pressure may also exist.

Similar to shock-scattering histotripsy, the large boiling bubble within the focal zone can act to scatter the incident shock wave. Indeed, a structured bubble cloud akin to that documented in shock-scattering histotripsy has been observed to form proximal to the boiling bubble (Fig. 9) (Khokhlova et al. 2011; Pahk et al. 2017). The layers of the bubble cloud were separated by λ/2. Numerical calculations of the interactions of shock waves with bubbles 100–500 μm in diameter confirm that regions of constructive interference occur at a distance of λ/2 from the bubble (Pahk et al. 2017). The discrete layering of the bubble cloud in boiling histotripsy differs from the bubble cloud layering observed in shock-scattering histotripsy due to variations in the amplitude and degree of nonlinearity between the insonation schemes.

While shock-scattering cavitation can occur during boiling histotripsy, boiling is unlikely during intrinsic-threshold or shock-scattering histotripsy. For a 1-MHz fundamental frequency insonation, shock amplitudes in the range of 7 to 16 GPa would be required to initiate boiling during a shock-scattering histotripsy pulse based on Eq. (5). Even at an elevated temperature (*e.g.* thermal HIFU used in combination with histotripsy), boiling during a shock-scattering histotripsy pulse is unlikely when the initial medium temperature is less than 99°C (Fig 8B).

Bubble dynamics modeling

In order to predict the histotripsy-induced cavitation dynamics, and therefore the potential for tissue liquefaction, a Rayleigh-Plesset-like equation can be solved with a histotripsy excitation forcing function $p_a(t)$:

$$R\ddot{R} + \frac{3}{2}\dot{R}^2 = \left[\left(p_0 + \frac{2\sigma}{R_0} - p_v\right)\left(\frac{R_0}{R}\right)^{3\kappa} + p_v - \frac{2\sigma}{R} - \frac{4\eta\dot{R}}{R} - p_0 - p_a(t)\right]/\rho \quad (6)$$

where the diacritic dot denotes the temporal derivative. Detailed derivation of the Rayleigh-Plesset equation, as well as derivation of modified models which incorporate fluid compressibility, are provided elsewhere (Flynn 1964; Leighton 1994; Prosperetti and Lezzi 1986). For histotripsy-induced cavitation, the Rayleigh-Plesset model should be extended to incorporate the effects of elasticity to mimic a viscoelastic tissue. An early version of bubble oscillations in viscoelastic medium were modeled with linearized Kelvin-Voight elasticity

Author Manuscript Author Manuscript Author Manuscript Author Manuscript

(Yang and Church 2005). Calculations based on the Kelvin-Voight elastic model have been shown to be in qualitative agreement with experimental observations of shock scattering-induced bubble behavior (Bader and Holland 2016). Further refinement of the elastic model through incorporation of a finite-strain neo-Hookean elasticity (Vlaisavljevich et al. 2015c; Vlaisavljevich et al. 2016d) or the strain-hardening Fung elastic model (Movahed et al. 2016) have also been shown to be in qualitative agreement with experimental observations.

In general, the highly nonlinear nature of the Rayleigh-Plesset equation necessitates numerical solutions, and bubble expansion by histotripsy pulses has been explored numerically by several groups (Bader and Holland 2016; Mancia et al. 2017; Maxwell et al. 2013; Movahed et al. 2016; Vlaisavljevich et al. 2015c; Pahk et al. 2015). The tensions well in excess of the Blake threshold for histotripsy pulses simplifies the Rayleigh-Plesset equation significantly, and the maximum bubble size can be predicted with high accuracy for a single-cycle excitation analytically (Bader and Holland 2016):

$$R_{MAX} = \left[R_0 + \sqrt{\frac{2\mathrm{P}_0 p_0 \xi}{9\rho}}\tau\right]\left[\frac{\xi p_0 \mathrm{P}_0}{3p_{EFF}} + 1\right]^{1/3} \quad (7)$$

where ξ and τ are defined in Holland and Apfel (1989). The effects of surface tension, viscosity, and inertia are accounted for in Eq. (7). The analytic model has also been extended to account for finite-strain and strain-hardening media (Bader 2018).

In addition to its simplicity, the analytic model provides a means to identify appropriate contributions of the insonation scheme and medium properties to the overall bubble dynamics. The parameter τ denotes duration for forced bubble expansion, and can be expressed as $1/f$ when the peak negative pressure is much greater than the Blake threshold (Leighton 1994). The limiting value for τ indicates the maximum bubble size is inversely proportional to the fundamental frequency of the insonation, consistent with experimental observation (Vlaisavljevich et al. 2015c). The time-averaged pressure experienced by the bubble during its growth phase is expressed as $p_0\xi/3$. The term p_{EFF} in Eq. (7) represents the effective overpressure that arrests bubble growth after tension is no longer applied. The form of the effective pressure depends on the insonation type, as the contribution of compressional components vary between histotripsy insonation schemes. For a shock-scattering histotripsy pulse, the maximum bubble size depends roughly on the square root of the peak negative pressure due to the form of the effective pressure. In contrast, the bubble size increases nearly linearly with the peak negative pressure for intrinsic threshold excitations. These results indicate that nuclei grow larger by intrinsic threshold insonations compared to a shock-scattering histotripsy pulse.

Care should be taken when applying Eq. (7) to predict bubble growth. The pressure experienced by the bubble is assumed based on a pre-defined peak negative pressure, whereas the maximum bubble diameter saturates when the applied tension exceeds the intrinsic medium threshold, as discussed in Section **V.A** (Vlaisavljevich et al. 2015c). For shock-scattering histotripsy, Eq. (7) only predicts the growth of a bubble during the first cycle of the pulse. Beyond the first cycle, the growth rate of the bubble will decrease and

Author Manuscript Author Manuscript Author Manuscript Author Manuscript

depends on the time-averaged acoustic pressure. These analytic computations can be utilized to estimate the onset of shock scattering through classical scattering theory (Anderson 1950), and the axial extent of the cavitation based on the known shock scattering-induced bubble cloud growth rate (Bader and Holland 2016).

Medium properties that influence the bubble dynamics

For histotripsy excitations, the maximum bubble size is relatively independent of the medium surface tension (Bader and Holland 2016; Maxwell et al. 2013). The medium viscosity and elasticity contribute to the degree of bubble expansion. Indeed, a significant reduction in the maximum bubble diameter has been observed in *in vitro* agar phantoms with increasing Young's modulus over the range of 0 (water) to 570 kPa (Vlaisavljevich et al. 2015c). For a given elasticity, a lower frequency excitation resulted in larger bubble expansion due to extended duration of the tensile phase, as depicted in Fig. 10. However, the threshold for bubble nucleation with single-cycle pulses was nearly independent of the tissue stiffness and the insonation frequency (Vlaisavljevich et al. 2015b).

While medium stiffness has ramifications for the microscale bubble dynamics, it has minimal contribution to the intrinsic threshold. This is reflected in the pressure at the bubble wall due to medium properties during the bubble oscillation. Surface tension and viscous pressure terms are inversely proportional to the bubble size, and decrease as the bubble undergoes massive expansion (Fig. 11). The elastic pressure contribution for a finite-strain elastic model, however, approaches a maximum value when the bubble size is much larger than that of the nucleus (Gent 1996). The elastic pressure term therefore acts as an additional overpressure to suppress bubble growth, thereby reducing the maximum bubble diameter.

Sustained bubble dynamics

The discussion thus far has focused on the bubble behavior over the course of a single ultrasound pulse. Tissue ablation requires the application of tens to hundreds of pulses for complete liquefaction of the focal zone (Wang et al. 2012). For all forms of histotripsy, bubbles appear to persist well after the application of the histotripsy pulse. Remnants of bubble clouds have been observed optically up to 30 ms after the therapeutic excitation (Prieur et al. 2015; Xu et al. 2007a), and up to 50 ms post insonation acoustically (Bader et al. 2018). A potential cause of these persistent bubble clouds is gas diffusion during bubble expansion (Bader and Bollen 2018). The infiltration of gas dissolve in the medium into the bubble will increase its equilibrium size, thereby slowing the passive dissolution process (Church 1989). Fragmentation of the bubble during an inertial collapse can also proliferate daughter bubbles (Leighton 1995). The remnant nuclei produce a 'memory effect', whereby bubbles at the same physical location are repeatedly excited and a similar structure of the cloud appears from pulse-to-pulse.

The peak negative pressure necessary to produce inertial cavitation with a subsequent pulse is lowered in the presence of a remnant bubble cloud (Xu et al. 2007a). The reduced threshold for persistent bubble clouds has been utilized for strategies of tissue erosion by applying a higher amplitude 'bubble cloud initiating' pulse following by lower amplitude 'maintenance' pulses (Xu et al. 2006b). The expansion of bubbles within the cloud shields

Author Manuscript Author Manuscript Author Manuscript Author Manuscript

the acoustic pulse from the focal zone, with the nuclei closest to the transducer undergoing greater expansion than those in the distal part of the focus. The asymmetric axial expansion produce a comet-shaped head and tail of the bubble cloud.

With each pulse, bubble activity contributes to the eventual mechanical breakdown of the tissue. Cellular stress/strain via bubble oscillations appears to be a primary mechanism of histotripsy-induced ablation (Vlaisavljevich et al. 2016d). Other mechanisms, such as acoustic atomization (Simon et al. 2012), may also contribute to tissue break down. The necessary strain to rupture a cell is a function of time of the applied strain (Hategan et al. 2003; Li et al. 2013). Large cellular deformations (more than 150% stretching) are generated in the presence of histotripsy bubbles (Vlaisavljevich et al. 2016d). While cells in the proximity of the bubble appear to be lysed within the first pulse, cell bisection or complete removal at the edge of the focal zone occurs over the course of several pulses. Thus sustained activity throughout the focal zone is the hallmark for complete liquefaction of the target tissue (Vlaisavljevich et al. 2016d).

Insonation of residual bubbles causes strain at discrete location within the focal zone during a pulse, but incomplete liquefaction of the target tissue (Wang et al. 2012). Lesions may progress towards complete disintegration through several potential means. New nuclei within the cloud may be excited, causing damage in new locations (Maxwell et al. 2010b). Bubbles in the same location may damage their surroundings, and their dynamics change from pulse to pulse to grow and damage a greater area (Movahed et al. 2017). A third possibility is that the remnant nuclei undergo translational motion between pulses, progressing the spatial extent of damage.

Changes in the sustained bubble dynamics occur in boiling histotripsy as well. The onset of boiling is dependent on the number of applied pulses. Boiling coincides with the predicted time to boil for a single pulse (Canney et al. 2010), but occurs prior to the predicted time in subsequent pulses (Khokhlova et al. 2011). The reduction in the time to boil can be attributed to heat deposition between pulses, despite the relatively low pulse repetition frequency (1 Hz, 0.01 duty factor). Over the course of the therapeutic application, the extent of the boiling bubbles encompasses the focal volume.

Amendments to Apfel’s golden rules

In this section, ongoing and proposed studies are discussed for promoting tissue-stressing bubble activity through the manipulation of the acoustic parameters, nucleation environment, and monitoring the histotripsy process. These processes are proposed as modification of Apfel’s golden rules to accentuate histotripsy-induced cavitation activity: Change thy sound field, change thy liquid, and quantify when everything happens.

Change thy sound field

One approach to improve histotripsy therapy for various clinical applications is to modulate the applied acoustic field to control histotripsy-induced bubble dynamics. Boiling and shock-scattering histotripsy rely on multiple processes to induce the bubble activity necessary for tissue fractionation. In contrast, nucleation through tensile-only pulses is a

Author Manuscript Author Manuscript Author Manuscript Author Manuscript

single process. The bubble cloud dimensions (size, shape, location, bubble density) can be predictably changed by altering the geometry of the therapy transducer (Vlaisavljevich et al. 2017a). Furthermore, a stochastic model can be used to predict the lesion dimensions for a given ultrasound field and number of pulses applied to a region (Lin et al. 2014b; Maxwell et al. 2013). Such modeling provides a theoretical basis for design of devices and therapy planning in the intrinsic threshold regime.

Dual-frequency transducers for intrinsic nucleation allow the targeting of deep tissue targets (Lin et al. 2015) or incitation of specific bubble behaviors (Vlaisavljevich et al. 2015c). By using a multi-frequency source, nearly monopolar waveforms with a single compression or tension phase can be generated in the focus (Lin et al. 2014a). No appreciable mechanical effects are produced for 100 MPa monopolar compressive pulses, while tensile monopolar pulses with peak negative pressure of 30 MPa consistently nucleated bubble clouds in tissue-mimicking phantoms. Monopolar pulses may have advantages for histotripsy therapy applications, such as more precise bubble cloud generation due to decreased nucleation through scattering, and a reduced thermal profile. Additionally, monopolar excitations can be utilized as a tool to investigate the underlying histotripsy nucleation processes (Vlaisavljevich et al. 2016b).

Although intrinsic-threshold histotripsy represents the most predictable form of histotripsy therapy, it is often not feasible to generate the tension necessary for intrinsic nucleation. Multiple cycle acoustic pulses can be used to generate shock-scattering or boiling histotripsy bubble clouds at tensions less than the intrinsic threshold. The dependence of the shock-scattering bubble cloud formation on the insonation parameters (e.g. pulse repetition frequency, degree of nonlinearity, pulse duration, etc.) (Maxwell et al. 2011b; Vlaisavljevich et al. 2014) indicate pulsing strategies can be optimized for tissue ablation. Yoshizawa *et al.* devised a two-step amplifier that enhances shock scattering by controlling the degree of nonlinear waveform distortion (Yoshizawa et al. 2012). Another insonation scheme from the same group employed negative-enhanced or positive-enhanced pulses to promote sparse bubble growth or shock scattering, respectively. Bubble clouds were readily nucleated with insonation schemes of negative-enhanced pulses followed by positive-enhanced pulses. When the order was reversed, bubble cloud formation was suppressed due to a lack of initial scatterers from the negative-enhanced wave. These shock-induced bubble clouds were used to enhance thermal HIFU heating.

Frequency is another parameter that should be considered for efficacious tissue fractionation. The intrinsic threshold is not strongly dependent on the driving frequency (Vlaisavljevich et al. 2015b). However, the maximum bubble size, and therefore extent of strain-induced damage (Bader 2018), is inversely proportional to frequency (Fig. 10). Other variables, such as the bubble dynamics, rate and effectiveness of ablation, potential for collateral damage, target depth, and prefocal cavitation are all affected by the choice of frequency. The choice of histotripsy insonation frequency should therefore weigh the likelihood of inducing the intended bubble activity with these potential undesirable outcomes.

Author Manuscript Author Manuscript Author Manuscript Author Manuscript

Sustaining the mechanical activity necessary for histotripsy-induced ablation requires the activation of intrinsic nuclei for each histotripsy pulse. The primary limitation in activating new intrinsic nuclei are bubble clouds that persist between pulses (Xu et al. 2007a). Insonation of these extrinsic nuclei causes strain at discrete locations within the focal zone and incomplete liquefaction of the target tissue (Wang et al. 2012). Pulse repetition frequencies of 1 to 10 Hz are required to allow complete dissolution of bubbles between excitations (Maxwell et al. 2013; Wang et al. 2012). Histotripsy treatment planning thus requires a compromise between efficacy and duration. Low-amplitude 'bubble deleting' pulses interleaved with histotripsy pulses have shown promise to remove residual bubbles in both *in vitro* phantom studies (Duryea et al. 2015) and model urinary stones (Roberts et al. 2015). Bubble deleting pulses may act to force bubble coalescence through secondary-Bjerknes forces (Duryea et al. 2014), with the large bubbles rising under buoyancy out of the focal zone. Alternatively, the bubble deleting pulses may force the residual bubbles into different parts of the tissue via primary Bjerknes forces, allowing uniform bubble activity throughout the focal zone (Acconcia et al. 2013).

Change thy liquid

Another approach to enhancing histotripsy is the modulation of nuclei within the target tissue through the introduction of exogenous agents (Fig. 12). Ultrasound contrast microbubbles were utilized in the earliest formulations of histotripsy to enhance cavitation activity (Tran et al. 2003). While microbubbles can enhance the efficacy of ablation with focused ultrasound sources (McDannold et al. 2016; McDannold et al. 2013; McDannold et al. 2006) and display similar histotripsy-induced dynamics to that of intrinsic nuclei (Bader et al. 2016b), bubble nucleation would be restricted to vasculature (Kwan et al. 2015). Exogenous nuclei reduce the threshold for histotripsy-induced bubble nucleation (Vlaisavljevich et al. 2013a), thereby reducing the overall bubble size (Bader 2018). The change in bubble dynamics with exogenous nuclei consequently reduces the efficacy of tissue ablation (Vlaisavljevich et al. 2016a). Microbubbles are no longer necessary to generate cavitation due to the advances in histotripsy transducer and amplifier technology (Hall and Cain 2006). However, there remain some potential advantages of using exogenous agents for targeted ablation.

Nanodroplets have been explored for several years as a means to induce acoustically-driven cavitation (Kripfgans et al. 2000). Nanodroplets are composed of a metastable perfluorocarbon liquid surrounded by a stabilizing shell. A high-amplitude acoustic pressure transitions the liquid to a gas, producing a histotripsy-friendly bubble (Fig. 13) (Apfel and Roy 1983; Radhakrishnan et al. 2016). Formulations of nanodroplets specifically to target micro-metastases were developed (Yuksel Durmaz et al. 2014) and tested *in vitro*. Initial studies found a significant decrease in the threshold for bubble cloud formation with ~200 nm diameter nanodroplets (~10 MPa) compared to without the droplets (~28 MPa) for 500-kHz insonations (Vlaisavljevich et al. 2013a). The microtripsy-mediated droplet transition threshold increases with frequency (Vlaisavljevich et al. 2015a), in contrast to measurements with non-histotripsy insonations (Kripfgans et al. 2000). For nanodroplet-mediated histotripsy (NMH), homogenous nucleation of the perfluorocarbon liquid occurs via homogenous tensile nucleation (Vlaisavljevich et al. 2015a), whereas heating via

Author Manuscript Author Manuscript Author Manuscript Author Manuscript

superharmonic focusing is a mechanism for non-histotripsy droplet transition (Li et al. 2014a; Shpak et al. 2013). Liquefaction of agar phantoms (Vlaisavljevich et al. 2013a) and cancer tumor spheroids (Aydin et al. 2016) can be achieved with NMH. A larger number of pulses is required for complete liquefaction of the focal zone is required for NMH compare to insonation without droplets, indicating smaller size for bubbles nucleated from droplets compared to intrinsic nuclei. Sustainable droplet nucleation is dependent on the boiling temperature of the perfluorocarbon (Vlaisavljevich et al. 2016a). At peak negative pressures above the threshold for bubble cloud formation, cavitation is only sustained for 10 pulses for droplets formed with perfluoropentane (boiling point of 29°C). Robust bubble clouds were observed for droplets formed with perfluorohexane (boiling point of 56°C) up to 1000 pulses, likely due to re-condensing of the gas into a liquid. Thus, higher boiling point perfluorocarbon droplets have an advantage for sustained NMH ablation.

Echogenic liposomes (ELIP) are theragnostic agents that can be functionalized for targeted ultrasound contrast (Tiukinhoy-Laing et al. 2007) and localized drug delivery (Shaw et al. 2009; Smith et al. 2010). Gas microbubbles entrained within ELIP can act as cavitation nuclei (Bader et al. 2015b), and may serve as sites for shock scattering to initiate bubble cloud formation (Tran et al. 2003). Thrombolytic-loaded ELIP with octafluoropropane gas microbubbles (OFP t-ELIP) were utilized to test the efficacy of clot lysis in combination with histotripsy (Bader et al. 2016b). An improvement in thrombolytic efficacy was observed for the combination of histotripsy and OFP t-ELIP compared to histotripsy alone. The degree of cavitation activity was similar when comparing treatment arms with and without OFP t-ELIP.

An alternative scheme for exogenous nucleation is to stabilize gas within motes on hydrophobic particles (Apfel 1970b; Crum 1979). Through an interfacial seed polymerization method (Okubo et al. 2001), nanocups have been manufactured from polystyrene spheres (Kwan et al. 2015). The hydrophobic surface of the nanocup harbors a gaseous core that will undergo inertial cavitation at peak negative pressures between 0.5-1 MPa (Kwan et al. 2015). Due to their relatively small size compared to microbubbles (100-500 nm versus 0.6-10 μm) (Graham et al. 2014), nanocups and droplets can efficiently penetrate leaky tumor vasculature (Kwan et al. 2015). Other potential applications for nanocups include transdermal transport of vaccines (Bhatnagar et al. 2016) and delivery of oncolytic vaccinia viruses (Myers et al. 2016).

In addition to adding exogenous nuclei, the nucleability of a medium can be altered through temperature considerations. Heating reduces tissue stiffness through the denaturing of collagen and other proteins, particularly in tissue resistant to mechanical activation (Vlaisavljevich et al. 2015d). Stiff tissues naturally resistant to histotripsy can be softened via heating in order to enhance their susceptibility to histotripsy-induced mechanical damage. Thermal pretreatment can also be used for reducing the nucleation pressure required for generating microtripsy bubble clouds (Vlaisavljevich et al. 2016e), with these two approaches likely complementing each other. Similar changes in the tissue occur during boiling histotripsy, as a small section of the tissue near the center of the focus is heated to at least 100°C.

Author Manuscript Author Manuscript Author Manuscript Author Manuscript

Quantify when everything happens

The final means to improve histotripsy therapy is the advancement of image guidance methods. B-mode echogenicity is the most ubiquitous parameter for histotripsy image guidance and assessment of treatment efficacy (Hall et al. 2007a). The bubble cloud appears hyperechoic on a B-mode ultrasound image, while liquefied tissue appears hypoechoic (Fig. 1) (Hall et al. 2007a; Hall et al. 2005). A significant variability between subjects has been noted, preventing quantification of B-mode images (Hall et al. 2007a). This has prompted testing alternative imaging modalities for histotripsy. Theses imaging methods can be categorized as real-time assessment of bubble activity for image guidance (Fig. 14), or assessment of the treatment efficacy through bubble-mediated changes in tissue structure.

Quantify bubble activity

There is some advantage to quantifying bubble cloud activity during insonation, as the morphology of the liquefaction zone changes with time (Vlaisavljevich et al. 2016c) and the immediate physiologic responses may mask imaging assessment of ablation zone extent (Zhou 2011). For thermal ablation, MR thermometry can be utilized to generate maps of thermal dose to estimate the therapeutic efficacy *in situ* (Rieke and Butts Pauly 2008). Histotripsy pulses cause minimal tissue heating (Kieran et al. 2007), and an equivalent means to monitor the “mechanical dose” of the therapy is required. During the oscillation of a bubble, a portion of the mechanical work is transformed into acoustic emissions (Leighton 1994). Acoustic emissions can serve as a surrogate for the mechanical action of cavitation (Bader et al. 2012a), and to quantify the type of bubble activity. Stable cavitation can be characterized by acoustic emissions containing harmonics of the fundamental, as well as rational fractions known as sub- and ultraharmonics (Bader and Holland 2012; Hitchcock et al. 2011; O’Reilly and Hynynen 2012). An inertially collapsing bubble generates broadband acoustic emissions (Haworth et al. 2017). Histotripsy-induced bubble clouds produce harmonics (Bader et al. 2016b) and broadband (Canney et al. 2010; Vlaisavljevich et al. 2015b) emissions during the acoustic excitation. The presence of harmonics in the acoustic spectra may be indicative of geometric scattering of the nonlinear histotripsy excitation by the bubble cloud (Maxwell et al. 2011b). After the acoustic excitation, shock waves are generated by the inertial collapse of the bubble cloud (Macoskey et al. 2018; Maxwell et al. 2013).

The primary means of detecting stable (Bader et al. 2015c; Sun et al. 2017) and inertial (Desjouy et al. 2013; Hockham et al.) cavitation are single element transducers. Backscattered emissions have been recorded with single element transducers during intrinsic-threshold (Maxwell et al. 2013; Vlaisavljevich et al. 2015b), shock-scattering (Xu et al. 2005), and boiling (Canney et al. 2010) histotripsy excitations. A limitation of single-element transducers is the inability to triangulate bubble activity. Passive cavitation imaging (PCI) utilizes an ultrasound imaging array to detect and beamform acoustic emissions generated by the mechanical oscillations of bubbles (Gyongy et al. 2008; Salgaonkar et al. 2009). The resultant image maps cavitation activity spatially, and has been explored *in vitro* and *in vivo* to monitor thermal ablation with focused ultrasound (Arvanitis and McDannold 2013; Haworth et al. 2015; Jensen et al. 2012) and ultrasound-mediated drug delivery in real time (Choi et al. 2014; Coviello et al. 2015; Haworth et al. 2016; Kwan et al. 2015).

Author Manuscript Author Manuscript Author Manuscript Author Manuscript

Histotripsy bubble clouds have been monitored with PCI during liquefaction of a clot *in vitro* (Bader et al. 2016b). The spatial location of acoustic power recorded with PCI and grayscale recorded with plane wave B-mode imaging have been compared to the location of liquefaction in a prostate tissue phantom (Bader et al. 2018) (Fig. 15). Passive cavitation imaging had a better area under the receiver operator characteristic, accuracy, sensitivity, and negative predictive value for phantom liquefaction than plane wave B-mode imaging. However, B-mode and PCI were only compared to the phantom along the central axis of the histotripsy source (azimuth of the imaging array) due to the limited range resolution of the delay, sum, and integrate beamformer used to process the passive images (Coviello et al. 2015). One means to improve the range resolution of PCI is to modify the geometry of the passive receiver array (Jones et al. 2018; O'Reilly et al. 2014). Elements within a hemispherical histotripsy source have been utilized to localize intrinsic threshold-induced cavitation, including quantifying the onset of bubble expansion and collapse (Macoskey et al. 2017). The limited bandwidth of the passive receivers prevented meaningful frequency analysis of the emissions (thereby the type of mechanical action), though this could be improved through the use of broadband receivers.

A limitation of the use of acoustic emissions to quantify bubble activity is the difficulty in system-independent cavitation emission measurements. Good agreement has been observed in the measured emission spectra and that predicted via the Yang/Church model for a single bubble (Collin and Coussios 2011). These results rely on careful calibration of the passive detector, with full knowledge of the spatial- and frequency-dependent sensitivity (Rich and Mast 2015a). The calibration accuracy of passive detectors is reduced in the presence of multiple emission sources characteristic of a histotripsy-generated bubble cloud (Rich and Mast 2015b). These calibration methods also assume spherical spreading of the emissions (Sboros et al. 2005), whereas scatter from histotripsy-generated bubble clouds have an angular dependence (Bader et al. 2018). The angular dependence of emissions may be imaged through the use of multi-element passive arrays (Haworth et al. 2017), but more work is still needed to quantify arbitrary cavitation emission source geometries.

Diagnostic ultrasound offers an improved temporal and spatial resolution compared to MR imaging at a reduced healthcare cost. But diagnostic ultrasound is inherently a two-dimensional imaging modality, cannot penetrate boney structures, and lacks the soft-tissue contrast compared to MR. Particularly for transcranial applications, MR imaging is important for histotripsy image guidance. Bubble clouds have been visualized with MR imaging (Allen et al. 2014; Allen et al. 2015). A sharp increase in the attenuation factor of gradient echo sequences was detected for insonation of an agar phantom between 24 and 28 MPa for intrinsic-threshold histotripsy pulses (Allen et al. 2014), indicating bubble cloud formation at peak negative pressures consistent with previous observations (Maxwell et al. 2013). These early findings indicate the timing between the therapy pulse and the imaging gradients are critical for monitoring cavitation. In a follow up study in *ex vivo* tissue, these sequences were tested against acoustic emissions recorded with a passive cavitation detector (Allen et al. 2015). While there was agreement between the two methods on the cavitation threshold, the MR sequences were not as sensitive to bubble cloud formation compared to acoustic methods due to partial volume effects associated with MR imaging. These findings were based on 1-D MR scans, but can be extended to additional dimensions.

Author Manuscript Author Manuscript Author Manuscript Author Manuscript

In addition to volumetric oscillations, histotripsy-nucleated bubbles translate under primary radiation force in liquefied tissue (Xu et al. 2007). Monitoring bubble cloud motion has been studied as a means to quantify tissue liquefaction. Color Doppler, which is sensitive to bubble motion (Ernst et al. 1996; Jauss and Zanette 2000), was found to be highly accurate for monitoring bubble cloud-induced fluid motion when compared to particle velocity imaging (Maxwell et al. 2014; Miller et al. 2016). Tissue motion around the bubble cloud was found to be chaotic immediately following insonation, after which coherent motion was observed. Movement was initially towards the source, but then reversed direction. The change in tissue direction may be due to a strong, symmetric collapse of the bubble cloud several milliseconds after the histotripsy pulse (Prieur et al. 2015; Xu et al. 2007b). A significant correlation was observed between the time required for the coherent motion to reverse and liquefaction of a fibrin clot *in vitro* (Zhang et al. 2015) and *ex vivo*> porcine liver (Miller et al. 2016). While these studies employed color Doppler (Szabo 2004), which is sensitive to the change in size of the bubble cloud post excitation, additional information about the nonlinear response of the bubble cloud can be extracted from pulse inversion Doppler (Li et al. 2014c). A combination of these techniques could be helpful in quantifying the bubble cloud activity, distribution of bubbles, and degree of tissue liquefaction. Tissue motion during treatment may result in artifacts of bubble-induced color Doppler, and limit its accuracy during *in vivo* use.

Quantify changes in the medium due to bubble activity

While monitoring bubble activity is useful for image guidance, the clinical endpoint for histotripsy therapy is tissue liquefaction. To gauge the treatment efficacy, it is critical to assess bubble dose-dependent changes in tissue structure. Ultrasound elastography has been investigated to assess the change in tissue stiffness over the course of histotripsy therapy. Tissue fractionation occurs over the application of tens to hundreds of histotripsy pulses. A strong decrease in tissue elasticity occurs as fractionation ensues (Hall et al. 2012) that can be visualized with acoustic radiation force imaging (ARFI) (Palmeri and Nightingale 2011). Changes in the Young's modulus of *ex vivo* tissue exposed to histotripsy have been shown to correlate with a decrease in the number of intact cellular nuclei (Wang et al. 2014). Furthermore, ARFI is more sensitive to tissue fractionation than B-mode hypoechogenicity. As the tissue liquefies, visualization of the shear waves generated in the ARFI sequence becomes difficult in the hypoechoic focal zone. As such, the accuracy of elastography techniques for delineating the liquefaction zone may decrease during the final stages of the treatment.

In addition to diagnostic ultrasound modalities, histotripsy-induced liquefaction zones have been visualized with magnetic resonance (MR) imaging at field strengths between 7 and 9 T (Allen et al. 2014; Khokhlova et al. 2009; Allen et al. 2015; Vlaisavljevich et al. 2016c). Changes in the media structure have been clearly delineated with T2, Tl, diffusion weighted, and contrast enhanced sequences *in vitro* and *in vivo* (Allen et al. 2017; Smolock et al. 2018). The lesion appearance varies based on the tissue viability (*in vivo* vs. *ex vivo*), and the time at which the image is acquired relative to the histotripsy therapy. The MR pixel intensity within the focal zone increases immediately post liquefaction of *ex vivo* tissue (Allen et al. 2015; Kim et al. 2013; Vlaisavljevich et al. 2013b), but decreases immediately

Author Manuscript Author Manuscript Author Manuscript Author Manuscript

following *in vivo* insonation (Vlaisavljevich et al. 2016c). Over the first few days post treatment, the MR pixel intensity of the treatment zone increases relative to the background, suggesting iron-based blood products and edema within the lesion. The pixel intensity gradually decreases over time, and appears to be resolved within 28 days sans a thin rim (Vlaisavljevich et al. 2016c), indicating the accumulation of deoxygenated red blood cells (Kim et al. 2013). It was noted that histotripsy ablation zones could be clearly visualized immediately post insonation with T2-weighted imaging. Thermally generated ablation zones can require several weeks to be fully visible under T2 imaging, in contrast to histotripsy-generated lesions (Coad et al. 2003; Marrero and Pelletier 2006).

Conclusions

Over the course of this review, the salient features of histotripsy bubble activity have been distinguished from other forms of cavitation. While seemingly disparate insonation schemes are utilized in histotripsy, there remain unifying mechanisms and concepts that govern this specific type of bubble behavior. In particular, supplying sufficient tension to activate expansion of a ubiquitous population of bubble nuclei can produce consistent formation of bubbles in tissue. Intrinsic-threshold and shock-scattering histotripsy produce tension that exceed an intrinsic cavitation threshold of the medium at physiologic conditions. Experiments indicate that boiling histotripsy heats the medium rapidly, reducing the intrinsic threshold to a level near the incident peak negative pressure. Evidence that multiple types of nucleation can occur simultaneously (*e.g.* shock-scattering and boiling (Khokhlova et al. 2011)) confound complete discretization of histotripsy nucleation schemes.

The expansion of the nanoscale nuclei to bubbles tens of micrometers to millimeters serves as acting force of histotripsy therapy, imparting sufficient strain to lyse the surrounding cells and break up the extracellular components (Vlaisavljevich et al. 2016d). However, there still remain a gap in knowledge about the fractionation process. Qualitative correlations exist between bubble activity and bioeffects, but quantification of these relationships is still lacking. Strain induced by bubble volumetric oscillations has been shown to induce cell lysis (Vlaisavljevich et al. 2016d). Jetting, translation, and atomization have also been shown to occur during the histotripsy cavitation process. Which of these mechanisms are causal to tissue liquefaction and which are superfluous bubble activity (*e.g.* changes in bubble activity due to changes in the environment) remains unknown. The highly nonlinear action of cavitation also hampers straightforward identification of the appropriate parameter set for promotion of a specific bubble activity. There is no singular “knob” to adjust in order to engage bubble jetting, for instance. Further understanding of the interaction of histotripsy bubbles with the insonation source and their surrounding medium, as well as promotion of specific bubble activities associated with an intended bioeffect should remain active areas of research. Finally, image guidance methods are needed for feedback of the intended histotripsy-induced bubble activity. Despite these gaps in knowledge, the continual progress being made towards understanding bubble behavior in histotripsy has already revealed several reliable methods for tissue ablation with the potential to replace many surgical procedures in the future.

Author Manuscript Author Manuscript Author Manuscript Author Manuscript

Acknowledgements

This work was funded in part by the National Institutes of Health, through Grants K12 CA139160, R01 HL13334, KOI DK104854. Thanks to Dr. Christy Holland for sharing the echogenic liposome schematic.

References

Acconcia C, Leung BYC, Hynynen K, Goertz DE. Interactions between ultrasound stimulated microbubbles and fibrin clots. Appl Phys Lett 2013;103:053701.

Ainslie MA, Leighton TG. Review of scattering and extinction cross-sections, damping factors, and resonance frequencies of a spherical gas bubble. J Acoust Soc Am 2011;130:3184. [PubMed: 22087992]

Allen SP, Hall TL, Cain CA, Hernandez-Garcia L. Controlling cavitation-based image contrast in focused ultrasound histotripsy surgery. Magn Reson Med 2014;73:204–213. [PubMed: 24469922]

Allen SP, Hernandez-Garcia L, Cain CA, Hall TL. MR-based detection of individual histotripsy bubble clouds formed in tissues and phantoms. Magn Reson Med 2015;76:1486–1493. [PubMed: 26599823]

Allen SP, Vlaisavljevich E, Shi J, Hernandez-Garcia L, Cain CA, Xu Z, Hall TL. The response of MRI contrast parameters in in vitro tissues and tissue mimicking phantoms to fractionation by histotripsy. Phys Med Biol 2017;62:7167–7180. [PubMed: 28741596]

Anderson VC. Sound scattering from a fluid sphere. J Acoust Soc Am 1950; 22: 426.

Apfel RE. The Role of Impurities in Cavitation-Threshold Determination. J Acoust Soc Am 1970a; 48:1179–1186.

Apfel RE. The Role of Impurities in Cavitation?Threshold Determination. J Acoust Soc Am 1970b; 48:1179–1186.

Apfel RE. Acoustic cavitation prediction. J Acoust Soc Am 1981;69:1624–1633.

Apfel RE, Roy SC. Instrument to detect vapor nucleation of superheated drops. Rev Sci Instrum 1983;54:1397–1400.

Arvanitis CD, McDannold N. Integrated ultrasound and magnetic resonance imaging for simultaneous temperature and cavitation monitoring during focused ultrasound therapies. Med Phys 2013;40:112901–15. [PubMed: 24320468]

Arvengas A, Davitt K, Caupin F. Fiber optic probe hydrophone for the study of acoustic cavitation in water. Rev Sci Instrum 2011a;82:034904. [PubMed: 21456781]

Arvengas A, Herbert E, Cersoy S, Davitt K, Caupin F. Cavitation in Heavy Water and Other Liquids. J Phys Chem B 2011b;l 15:14240–14245.

Atchley AA, Frizzell LA, Apfel RE, Holland CK. Thresholds for cavitation produced in water by pulsed ultrasound. Ultrasonics 1988;26:280–285. [PubMed: 3407017]

Aydin O, Vlaisavljevich E, Yuksel Durmaz Y, Xu Z, ElSayed MEH. Noninvasive Ablation of Prostate Cancer Spheroids Using Acoustically-Activated Nanodroplets. Mol Pharmaceutics 2016;13:4054–4065.

Bader KB. The influence of medium elasticity on the prediction of histotripsy-induced bubble expansion and erythrocyte viability. Phys Med Biol 2018; 63: 095010. [PubMed: 29553049]

Bader KB, Bollen V. The influence of gas diffusion on bubble persistence in shock-scattering histotripsy. J Acoust Soc Am, 2018;143:EL481–EL486. [PubMed: 29960422]

Bader KB, Bouchoux G, Holland CK. Sonothrombolysis. Ad Exp Med Biol 2015a; 880: 339–362.

Bader KB, Bouchoux G, Peng T, Klegerman ME, McPherson DD, Holland CK. Thrombolytic efficacy and enzymatic activity of rt-PA-loaded echogenic liposomes. J Thromb Thrombolysis, 2015b; 40:144–155. [PubMed: 25829338]

Bader KB, Crowe MJ, Raymond JL, Holland CK. Effect of Frequency-Dependent Attenuation on Predicted Histotripsy Waveforms in Tissue-Mimicking Phantoms. Ultrasound Med Biol, 2016a; 42:1701–1705. [PubMed: 27108036]

Bader KB, Gruber MJ, Holland CK. Shaken and Stirred: Mechanisms of Ultrasound-Enhanced Thrombolysis. Ultrasound Med Biol, 2015c;41:187–196. [PubMed: 25438846]

Author Manuscript Author Manuscript Author Manuscript Author Manuscript

Bader KB, Haworth KJ, Maxwell AD, Holland CK. Post hoc analysis of passive cavitation imaging for classification of histotripsy-induced liquefaction in vitro. IEEE Trans Med Imaging 2018; 37:106–115. [PubMed: 28783627]

Bader KB, Haworth KJ, Shekhar H, Maxwell AD, Peng T, McPherson DD, Holland CK. Efficacy of histotripsy combined with rt-PA in vitro. Phys Med Biol 2016b;61:5253–5274. [PubMed: 27353199]

Bader KB, Holland CK. Gauging the likelihood of stable cavitation from ultrasound contrast agents. Phys Med Biol 2012;58:127–144. [PubMed: 23221109]

Bader KB, Holland CK. Predicting the growth of nanoscale nuclei by histotripsy pulses. Phys Med Biol 2016;: 2947–2966. [PubMed: 26988374]

Bader KB, Mobley J, Church CC, Gaitan DF. The effect of static pressure on the strength of inertial cavitation events. J Acoust Soc Am 2012a;132:2286. [PubMed: 23039425]

Bader KB, Raymond JL, Mobley J, Church CC, Felipe Gaitan D. The effect of static pressure on the inertial cavitation threshold. J Acoust Soc Am 2012b; 132:728. [PubMed: 22894195]

Bailey MR, Pishchalnikov YA, Sapozhnikov OA, Cleveland RO, McAteer JA, Miller NA, Pishchalnikova IV, Connors BA, Crum LA, Evan AP. Cavitation detection during shock-wave lithotripsy. Ultrasound Med Biol 2005;31:1245–1256. [PubMed: 16176791]

Behnke AR. Decompression sickness incident to deep sea diving and high altitude ascent Medicine 1945;24:381–402. [PubMed: 21007394]

Bessonova OV, Khokhlova VA, Bailey MR, Canney MS, Crum LA. Focusing of high power ultrasound beams and limiting values of shock wave parameters. Acoust Phys 2009;55:463–473. [PubMed: 20161349]

Bhatnagar S, Kwan JJ, Shah AR, Coussios C-C, Carlisle RC. Exploitation of sub-micron cavitation nuclei to enhance ultrasound-mediated transdermal transport and penetration of vaccines. J Control Release 2016;238:22–30. [PubMed: 27417040]

Bigelow TA, Thomas CL, Wu H, Itani KMF. Histotripsy Treatment of S. Aureus Biofilms on Surgical Mesh Samples Under Varying Scan Parameters. IEEE Trans Ultrason, Ferroelect, Freq Contr 2018; 65:1017–1024.

Blake FGJ. Onset of Cavitation in Liquids. Thesis (PHD)-HARVARD UNIVERSITY, 1949 Source: American Doctoral Dissertations, Source code: W1949, page: 0049 1949.

Briggs LJ. Limiting Negative Pressure of Water. J Appl Phys 1950;21:721–722.

Brujan E, Nahen K, Schmidt P, Vogel A. Dynamics of laser-induced cavitation bubbles near an elastic boundary. J Fluid Mech 2001;433:251–281.

Bruot N, Caupin F. Curvature Dependence of the Liquid-Vapor Surface Tension beyond the Tolman Approximation. Phys Rev Lett American Physical Society, 2016;116:693–5.

Bunkin NF, Kochergin AV, Lobeyev AV, Ninham BW, Vinogradova OI. Existence of charged submicrobubble clusters in polar liquids as revealed by correlation between optical cavitation and electrical conductivity. Colloid Surf 1996;110:207–212.

Bykov TV, Zeng XC. Statistical Mechanics of Surface Tension and Tolman Length of Dipolar Fluids J Phys ChemB 2001;105:11586–11594.

Canney MS, Khokhlova VA, Bessonova OV, Bailey MR, Crum LA. Shock-Induced Heating and Millisecond Boiling in Gels and Tissue Due to High Intensity Focused Ultrasound. Ultrasound Med Biol 2010;36:250–267. [PubMed: 20018433]

Carstensen EL, Gracewski S, Dalecki D. The search for cavitation in vivo. Ultrasound Med Biol 2000;26:1377–1385. [PubMed: 11179611]

Chaussy C, Thuroff S. High-intensity focused ultrasound in the management of prostate cancer. Exp Rev Med Dev 2014;7:209–217.

Choi JJ, Carlisle RC, Coviello C, Seymour L, Coussios C-C. Non-invasive and real-time passive acoustic mapping of ultrasound-mediated drug delivery. Phys Med Biol 2014;59:4861–4877. [PubMed: 25098262]

Church CC. Prediction of rectified diffusion during nonlinear bubble pulsations at biomedical frequencies J Acoust Soc Am 1988;83:2210–2217. [PubMed: 3411017]

Author Manuscript Author Manuscript Author Manuscript Author Manuscript

Church CC. A theoretical study of cavitation generated by an extracorporeal shock wave lithotripter J Acoust Soc Am 1989;86:215. [PubMed: 2754108]

Church CC. Spontaneous homogeneous nucleation, inertial cavitation and the safety of diagnostic ultrasound. Ultrasound Med Biol 2002;28:1349–1364. [PubMed: 12467862]

Coad JE, Kosari K, Humar A, Sielaff TD. Radiofrequency ablation causes “thermal fixation” of hepatocellular carcinoma: a post-liver transplant histopathologic study. Clin Trans 2003;17:377–384.

Coleman AJ, Choi MJ, Saunders JE. Detection of acoustic emission from cavitation in tissue during clinical extracorporeal lithotripsy. Ultrasound Med Biol 1996;22:1079–1087. [PubMed: 9004432]

Collin JRT, Coussios C-C. Quantitative observations of cavitation activity in a viscoelastic medium. J Acoust Soc Am 2011;130:3289–3296. [PubMed: 22088001]

Commander KW, Prosperetti A. Linear pressure waves in bubbly liquids: Comparison between theory and experiments. J Acoust Soc Am 1989;85:1–15.

Coussios C-C, Roy RA. Applications of Acoustics and Cavitation to Noninvasive Therapy and Drug Delivery. Annu Rev Fluid Mech 2008;40:395–420.

Couzens DCF, Trevena DH. Tensile failure of liquids under dynamic stressing. J Phys D Appl Phys 2002;7:2277–2287.

Coviello C, Kozick R, Choi J, Gyongy M, Jensen C, Smith PP, Coussios C-C. Passive acoustic mapping utilizing optimal beamforming in ultrasound therapy monitoring. J Acoust Soc Am 2015;137:2573–2585. [PubMed: 25994690]

Crum L Tensile Strength of Water. Nature 1979;278:148–149.

Crum LA, Bailey MR, Guan J, Hilmo PR, Kargl SG, Matula TJ, Sapozhnikov OA. Monitoring bubble growth in supersaturated blood and tissue ex vivoand the relevance to marine mammal bioeffects. Acoust Res Lett On 2005;6:214–220.

Curley SA. Radiofrequency Ablation of Malignant Liver Tumors. Oncol 2001;6:14–23.

Dalecki D, Child SZ, Raeman CH, Cox C, Carstensen EL. Ultrasonically induced lung hemorrhage in young swine. Ultrasound Med Biol 1997;23:777–781. [PubMed: 9253826]

Datta S, Coussios C-C, Ammi AY, Mast TD, de Courten-Myers GM, Holland CK. Ultrasound-Enhanced Thrombolysis Using Definity® as a Cavitation Nucleation Agent. Ultrasound Med Biol 2008;34:1421–1433. [PubMed: 18378380]

Desjouy C, Poizat A, Gilles B, Inserra C, Béra J-C. Control of inertial acoustic cavitation in pulsed sonication using a real-time feedback loop system. J Acoust Soc Am 2013;134:1640. [PubMed: 23927204]

Duryea AP, Cain CA, Tamaddoni HA, Roberts WW, Hall TL. Removal of residual nuclei following a cavitation event using low-amplitude ultrasound. IEEE Trans Ultrason, Ferroelect, Freq Contr IEEE, 2014;61:1619–1626.

Duryea AP, Roberts WW, Cain CA, Hall TL. Removal of residual cavitation nuclei to enhance histotripsy erosion of model urinary stones. IEEE Trans Ultrason, Ferroelect, Freq Contr IEEE, 2015;62:896–904.

Ernst H, Hahn EG, Balzer T, Schlief R, Heyder N. Color Doppler ultrasound of liver lesions: Signal enhancement after intravenous injection of the ultrasound contrast agent Levovist®. J Clin Ultrasound 1996;24:31–35. [PubMed: 8655665]

Fisher JC. The Fracture of Liquids. J Appl Phys 1948;19:1062–1067.

Flynn HG. Physics of Acoustic Cavitation in liquids In: Mason WP, ed. Physical Acoustics New York: Academic Press, Inc, 1964 pp. 58–172.

Fogazzi GB. Crystalluria: a neglected aspect of urinary sediment analysis. Nephrology Dialysis Transplantation 1996;11:379–387.

Fowlkes JB, Crum LA. Cavitation threshold measurements for microsecond length pulses of ultrasound. The Journal of the acoustical Society of America 1988;83:2190–2201. [PubMed: 3411016]

Freundlich H, Söllner K, Rogowski F. Einige Biologische Wirkungen von Ultraschallwellen. Klinische Wochenschrift 1932; 11:1512–1513.

Author Manuscript Author Manuscript Author Manuscript Author Manuscript

Fry FJ, Heimburger RF, Gibbons LV, Eggleton RC. Ultrasound for visualization and modification of brain tissue. Sonics and Ultrasonics, IEEE Trans Son Ultrason 1970; 17:165–169.

Fry WJ. Mechanism of Acoustic Absorption in Tissue. J Acoust Soc Am 1952;24:412–415.

Fry WJ, Fry FJ. Fundamental Neurological Research and Human Neurosurgery Using Intense Ultrasound. IRE Trans Med Electron 1960;ME-7:166–181. [PubMed: 13702332]

Fry WJ, Wulff VJ, Tucker D, Fry FJ. Physical Factors Involved in Ultrasonically Induced Changes in Living Systems: I. Identification of Non-Temperature Effects. J Acoust Soc Am 1950;22:867–876.

Gent AN. A New Constitutive Relation for Rubber. Rub Chem Technol 1996;69:59–61.

Gilling P Holmium Laser Enucleation of the Prostate (HoLEP). BJU International 2007;101:131–142.

Graham SM, Carlisle R, Choi JJ, Stevenson M, Shah AR, Myers RS, Fisher K, Peregrino M-B, Seymour L, Coussios C-C. Inertial cavitation to non-invasively trigger and monitor intratumoral release of drug from intravenously delivered liposomes. J Control Release The Authors, 2014;178:101–107.

Greenspan M, Tschiegg CE. Radiation-induced acoustic cavitation; apparatus and some results. J Res Nat Bur Stand 1967;71C:299.

Gruber MJ, Bader KB, Holland CK. Cavitation thresholds of contrast agents in an in vitro human clot model exposed to 120-kHz ultrasound. J Acoust Soc Am 2014;135:646–653. [PubMed: 25234874]

Gyongy M, Arora M, Noble JA, Coussios CC. Use of passive arrays for characterization and mapping of cavitation activity during HIFU exposure. IEEE Ultrasonics Symposium (IUS) IEEE, 2008 pp. 871–874.

ter Haar G, Coussios C. High intensity focused ultrasound: Physical principles and devices. Int J Hyperthermia 2007;23:89–104. [PubMed: 17578335]

ter Haar GR, Daniels S. Evidence for ultrasonically induced cavitation in vivo. Phys Med Biol 1981;26:1145–1149. [PubMed: 7323152]

Hall T, Cain C. A low cost compact 512 channel therapeutic ultrasound system for transcutaneous ultrasound surgery. AIP Conf Proc 2006;829:445.

Hall T, Fowlkes J, Cain C. A real-time measure of cavitation induced tissue disruption by ultrasound imaging backscatter reduction. IEEE Trans Ultrason, Ferroelect, Freq Contr 2007a;54:569–575.

Hall T, Fowlkes J, Cain C, Wang T-Y, Xu Z, Fowlkes JB, Cain CA, Hall TL. Imaging feedback of histotripsy treatments using ultrasound shear wave elastography. IEEE Trans Ultrason, Ferroelect, Freq Contr 2012;59:1167–1181.

Hall TL, Fowlkes JB, Cain CA. Imaging feedback of tissue liquefaction (histotripsy) in ultrasound surgery. IEEE Trans Ultrason, Ferroelect, Freq Contr 2005;3:1732–1734.

Hall TL, Hempel CR, Wojno K, Xu Z, Cain CA, Roberts WW. Histotripsy of the Prostate: Dose Effects in a Chronic Canine Model. Urol 2009;74:932–937. [PubMed: 19628261]

Hall TL, Kieran K, Ives K, Fowlkes JB, Cain CA, Roberts WW. Histotripsy of Rabbit Renal Tissue in Vivo: Temporal Histologic Trends. J Endourol 2007b;21:1159–1166. [PubMed: 17949317]

Hallaj IM, Cleveland RO. FDTD simulation of finite-amplitude pressure and temperature fields for biomedical ultrasound. J Acoust Soc Am 1999;105:L7. [PubMed: 10335650]

Haller J, Wilkens V, Shaw A. Determination of Acoustic Cavitation Probabilities and Thresholds Using a Single Focusing Transducer to Induce and Detect Acoustic Cavitation Events: I. Method and Terminology. Ultrasound Med Biol 2018;44:377–396. [PubMed: 29195754]

Hamilton MF, Blackstock DT. Nonlinear Acoustics. 1st ed San Diego, 1998.

Harr Ter GR, Daniels S, Morton K. Evidence for acoustic cavitation in vivo: Thresholds for bubble formation with 0.75-MHz continuous wave and pulsed beams. IEEE Trans. Ultrason., Ferroelect., Freq. Contr. IEEE transactions on …, 1986 pp. 162–164.

Harrell AG, Heniford BT. Minimally invasive abdominal surgery: lux et veritas past, present, and future. Am J Surg 2005;190:239–243. [PubMed: 16023438]

Harvey EN, Barnes DK, McElroy WD, Whiteley AH, Pease DC, Cooper KW. Bubble formation in animals. I. Physical factors. J Cell Comp Physiol 1944;24:1–22.

Harvey EN, Loomis AL. High frequency sound waves of small intensity and their biological effects. Nature 1928;121:622–624.

Author Manuscript Author Manuscript Author Manuscript Author Manuscript

Hategan A, Law R, Kahn S, Discher DE. Adhesively-Tensed Cell Membranes: Lysis Kinetics and Atomic Force Microscopy Probing. Biophys J 2003;85:2746–2759. [PubMed: 14507737]

Haworth KJ, Bader KB, Rich KT, Holland CK, Mast TD. Quantitative Frequency-Domain Passive Cavitation Imaging. IEEE Trans Ultrason, Ferroelect, Freq Contr 2017;64:177–191.

Haworth KJ, Raymond JL, Radhakrishnan K, Moody MR, Huang S-L, Peng T, Shekhar H, Klegerman ME, Kim H, McPherson DD, Holland CK. Trans-Stent B-Mode Ultrasound And Passive Cavitation Imaging. Ultrasound Med Biol 2016;42:518–527. [PubMed: 26547633]

Haworth KJ, Salgaonkar VA, Corregan NM, Holland CK, Mast TD. Using passive cavitation images to classify high-intensity focused ultrasound lesions. Ultrasound Med Biol 2015;41:2420–2434. [PubMed: 26051309]

Hempel CR, Hall TL, Cain CA, Fowlkes JB, Xu Z, Roberts WW. Histotripsy Fractionation of Prostate Tissue: Local Effects and Systemic Response in a Canine Model. J Urol 2011;185:1484–1489. [PubMed: 21334667]

Herbert E, Balibar S, Caupin F. Cavitation pressure in water. Phys Rev E 2006;74:041603.

Hitchcock KE, Ivancevich NM, Haworth KJ, Stamper DNC, Vela DC, Sutton JT, Pyne-Geithman GJ, Holland CK. Ultrasound-enhanced rt-PA Thrombolysis in an ex vivo Porcine Carotid Artery Model. Ultrasound Med Biol 2011;37:1240–1251. [PubMed: 21723448]

Hockham N, Coussios CC, Arora M. A real-time controller for sustaining thermally relevant acoustic cavitation during ultrasound therapy. IEEE Trans Ultrason, Ferroelect, Freq Contr 57:2685–2694.

Holland C, Deng C, Apfel R, Alderman J, Fernandez L, Taylor K. Direct evidence of cavitation in vivo from diagnostic ultrasound. Ultrasound Med Biol 1996;22:917–925. [PubMed: 8923710]

Holland CK, Apfel RE. Improved Theory for the Prediction of Microcavitation Thresholds. IEEE Trans Ultrason, Ferroelect, Freq Contr 1989;36:204–208.

Holt RG, Roy RA. Measurements of bubble-enhanced heating from focused, MHz-frequency ultrasound in a tissue-mimicking material. Ultrasound Med Biol 2001;27:1399–1412. [PubMed: 11731053]

Horiba T, Sano T, Ogaswara T, Takahira H. Observation of the growth of cavitation bubble cloud by the backscattering of focused ultrasound from a laser-induced bubble. 31st Int Congress High-Speed Imag Photon 2017; 10328: 1032819.

Hynynen K The threshold for thermally significant cavitation in dog's thigh muscle in vivo. Ultrasound Med Biol 1991; 17:157–169. [PubMed: 2053212]

Jaffray B Minimally invasive surgery. Arch Dis Child 2005;90:537–542. [PubMed: 15851444]

Jauss M, Zanette E. Detection of right-to-left shunt with ultrasound contrast agent and transcranial Doppler sonography. Cerebrovascular Diseases 2000;10:490–496. [PubMed: 11070388]

Jensen CR, Ritchie RW, Gyongy M, Collin JR, Leslie T, Coussios C-C. Spatiotemporal monitoring of high-intensity focused ultrasound therapy with passive acoustic mapping. Radiol 2012;262:252–261.

Johnsen E, Colonius T. Shock-induced collapse of a gas bubble in shockwave lithotripsy. J Acoust Soc Am 2008; 124:2011. [PubMed: 19062841]

Kennedy JE, Wu F, Haar ter GR, Gleeson FV, Phillips RR, Middleton MR, Cranston D. High-intensity focused ultrasound for the treatment of liver tumours. Ultrasonics 2004;42:931–935. [PubMed: 15047409]

Khokhlova TD, Canney MS, Khokhlova VA, Sapozhnikov OA, Crum LA, Bailey MR. Controlled tissue emulsification produced by high intensity focused ultrasound shock waves and millisecond boiling. J Acoust Soc Am 2011;130:3498. [PubMed: 22088025]

Khokhlova TD, Canney MS, Lee D, Marro KI, Crum LA, Khokhlova VA, Bailey MR. Magnetic resonance imaging of boiling induced by high intensity focused ultrasound. J Acoust Soc Am 2009;125:2420–2431. [PubMed: 19354416]

Khokhlova TD, Wang YN, Simon JC, Cunitz BW, Starr F, Paun M, Crum LA, Bailey MR, Khokhlova VA. Ultrasound-guided tissue fractionation by high intensity focused ultrasound in an in vivo porcine liver model. Proc Nat Acad Sci 2014;111:8161–8166. [PubMed: 24843132]

Khokhlova VA, Fowlkes JB, Roberts WW, Schade GR, Xu Z, Khokhlova TD, Hall TL, Maxwell AD, Wang Y-N, Cain CA. Histotripsy methods in mechanical disintegration of tissue: Towards clinical applications. Int J Hyperthermia 2015;31:145–162. [PubMed: 25707817]

Author Manuscript Author Manuscript Author Manuscript Author Manuscript

Kieran K, Hall TL, Parsons JE, Wolf JS Jr, Fowlkes JB, Cain CA, Roberts WW. Refining Histotripsy: Defining the Parameter Space for the Creation of Nonthermal Lesions With High Intensity, Pulsed Focused Ultrasound of the In Vitro Kidney. J Urol 2007; 178:672–676. [PubMed: 17574617]

Kim HC, Yang DM, Jin W, Ryu JK, Shin HC. Color Doppler Twinkling Artifacts in Various Conditions During Abdominal and Pelvic Sonography. J Ultrasound Med 2010;29:621–632. [PubMed: 20375381]

Kim Y, Fifer CG, Gelehrter SK, Owens GE, Berman DR, Vlaisavljevich E, Allen SP, Ladino-Torres MF, Xu Z. Original Contribution. Ultrasound Med Biol 2013;39:1047–1055. [PubMed: 23453378]

Kim Y, Hall TL, Xu Z, Cain CA. Transcranial histotripsy therapy: a feasibility study. IEEE Trans Ultrason, Ferroelect, Freq Contr 2014a;61:582–593.

Kim Y, Maxwell AD, Hall TL, Xu Z, Lin K-W, Cain CA. Rapid prototyping fabrication of focused ultrasound transducers. IEEE Trans Ultrason, Ferroelect, Freq Contr 2014b;61:1559–1574.

Kripfgans OD, Fowlkes JB, Miller DL, Eldevik OP. Acoustic droplet vaporization for therapeutic and diagnostic applications. Ultrasound Med Biol 2000;26:1177–1189. [PubMed: 11053753]

Kwan JJ, Myers R, Coviello CM, Graham SM, Shah AR, Stride E, Carlisle RC, Coussios C-C. Ultrasound-Propelled Nanocups for Drug Delivery. Small 2015; 11:5305–5314. [PubMed: 26296985]

Langevin P French Patent No. 505,703 (filed September 17, 1917; issued 8 5, 1920).

Leighton TG. The Acoustic Bubble. London: Academic Press, 1994.

Leighton TG. Bubble population phenomena in acoustic cavitation. Ultrason Sonochem 1995;2:S123–S136.

Leighton TG, Fedele F, Coleman AJ, McCarthy C, Ryves S, Hurrell AM, De Stefano A, White PR. A Passive Acoustic Device for Real-Time Monitoring of the Efficacy of Shockwave Lithotripsy Treatment. Ultrasound Med Biol 2008;34:1651–1665. [PubMed: 18562085]

Levin WP, Kooy H, Loeffler JS, DeLaney TF. Proton beam therapy. Br J Cancer 2005;93:849–854. [PubMed: 16189526]

Li DS, Kripfgans OD, Fabiilli ML, Brian Fowlkes J, Bull JL. Initial nucleation site formation due to acoustic droplet vaporization. Appl Phys Lett 2014a;104:063703–5. [PubMed: 24711671]

Li F, Chan CU, Ohl C-D. Yield Strength of Human Erythrocyte Membranes to Impulsive Stretching. Biophysi J 2013;105:872–879.

Li T, Chen H, Khokhlova T, Wang Y-N, Kreider W, He X, Hwang JH. Passive Cavitation Detection during Pulsed HIFU Exposures of Ex Vivo Tissues and In Vivo Mouse Pancreatic Tumors. Ultrasound Med Biol 2014b;40:1523–1534. [PubMed: 24613635]

Li T, Khokhlova T, Sapozhnikov O, O'Donnell M, Hwang J. A new active cavitation mapping technique for pulsed HIFU applications-bubble doppler. IEEE Trans Ultrason, Ferroelect, Freq Contr 2014c;61:1698–1708.

Li ZG, Xiong S, Chin LK, Ando K, Zhang JB, Liu AQ. Water's tensile strength measured using an optofluidic chip. Roy Soc Chem 2015;15:2158–2161.

Lin K-W, Hall TL, McGough RJ, Xu Z, Cain CA. Synthesis of monopolar ultrasound pulses for therapy: The frequency-compounding transducer. IEEE Trans Ultrason, Ferroelect, Freq Contr 2014a;61:1123–1136.

Lin K-W, Hall TL, Xu Z, Cain CA. Histotripsy Lesion Formation Using an Ultrasound Imaging Probe Enabled by a Low-Frequency Pump Transducer. Ultrasound Med Biol 2015;41:2148–2160. [PubMed: 25929995]

Lin KW, Kim Y, Maxwell A, Wang TY, Hall T. Histotripsy beyond the intrinsic cavitation threshold using very short ultrasound pulses: microtripsy. IEEE transactions on ultrasonics, ferroelectrics, and frequency control 2014b;61:251–265.

Lindquist C Gamma knife radiosurgery. Sem Rad Oncol 1995;5:197–202.

Lu DSK, Raman SS, Limanond P, Aziz D, Economou J, Busuttil R, Sayre J. Influence of Large Peritumoral Vessels on Outcome of Radiofrequency Ablation of Liver Tumors. J Vase Interv Radiol 2003;14:1267–1274.

Author Manuscript Author Manuscript Author Manuscript Author Manuscript

Lubner MG, Brace CL, Hinshaw JL, Lee FT. Microwave Tumor Ablation: Mechanism of Action, Clinical Results, and Devices. J Vase Interv Radiol 2010;21:S192–S203.

Macoskey JJ, Choi SW, Hall TL, Vlaisavljevich E, Lundt JE, Lee FTJ, Johnsen E, Cain CA, Xu Z. Using the cavitation collapse time to indicate the extent of histotripsy-induced tissue fractionation. Phys Med Biol 2018;63:055013 [PubMed: 29424711]

Macoskey JJ, Sukovich JR, Hall TL, Cain CA, Xu Z. Real-time acoustic-based feedback for histotripsy therapy. J Acoust Soc Am 2017;141:3551–3551.

Mancia L, Vlaisavljevich E, Xu Z, Johnsen E. Predicting Tissue Susceptibility to Mechanical Cavitation Damage in Therapeutic Ultrasound. Ultrasound Med Biol 2017;43:1421–1440. [PubMed: 28408061]

Marrero JA, Pelletier S. Hepatocellular Carcinoma. Clin Liver Dis 2006;10:339–351. [PubMed: 16971265]

Maxwell A, Sapozhnikov O, Bailey M, Crum L, Xu Z, Fowlkes B, Cain C, Khokhlova V. Disintegration of tissue using high intensity focused ultrasound: two approaches that utilize shock waves. Acoust Today 2012;8:24–37.

Maxwell AD, Cain CA, Duryea AP, Yuan L, Gurm HS, Xu Z. Noninvasive Thrombolysis Using Pulsed Ultrasound Cavitation Therapy – Histotripsy. Ultrasound Med Biol 2009;35:1982–1994. [PubMed: 19854563]

Maxwell AD, Cain CA, Fowlkes JB, Xu Z. Inception of cavitation clouds by scattered shockwaves. IEEE, 2010a;: 108–111.

Maxwell AD, Cain CA, Hall TL, Fowlkes JB, Xu Z. Probability of Cavitation for Single Ultrasound Pulses Applied to Tissues and Tissue-Mimicking Materials. Ultrasound Med Biol 2013;39:449–465. [PubMed: 23380152]

Maxwell AD, Owens G, Gurm HS, Ives K, Myers DD Jr, Xu Z. Noninvasive Treatment of Deep Venous Thrombosis Using Pulsed Ultrasound Cavitation Therapy (Histotripsy) in a Porcine Model. J Vase Interven Radiol 2011a;22:369–377.

Maxwell AD, Park S, Vaughan BL, Cain CA, Grotberg JB, Xu Z. Trapping of embolic particles in a vessel phantom by cavitation-enhanced acoustic streaming. Phys Med Biol 2014;59:4927–4943. [PubMed: 25109407]

Maxwell AD, Wang T-Y, Cain CA, Fowlkes JB, Sapozhnikov OA, Bailey MR, Xu Z. Cavitation clouds created by shock scattering from bubbles during histotripsy. J Acoust Soc Am 2011b; 130:1888. [PubMed: 21973343]

Maxwell AD, Wang TY, Yuan L, Duryea AP, Xu Z. A tissue phantom for visualization and measurement of ultrasound-induced cavitation damage. Ultrasound Med Biol 2010b;36:2132–2143. [PubMed: 21030142]

Maxwell AD, Yuldashev PV, Kreider W, Khokhlova TD, Schade GR, Hall TL, Sapozhnikov OA, Bailey MR, Khokhlova VA. A Prototype Therapy System for Transcutaneous Application of Boiling Histotripsy. IEEE Trans Ultrason, Ferroelect, Freq Contr 2017;: 1–.

McDannold N, Zhang Y, Vykhodtseva N. Nonthermal ablation in the rat brain using focused ultrasound and an ultrasound contrast agent: long-term effects. J Neurosurg 2016; 125:1539–1548. [PubMed: 26848919]

McDannold N, Zhang Y-Z, Power C, Jolesz F, Vykhodtseva N. Nonthermal ablation with microbubble-enhanced focused ultrasound close to the optic tract without affecting nerve function. J Neurosurg 2013; 119:1208–1220. [PubMed: 24010975]

McDannold NJ, Vykhodtseva NI, Hynynen K. Microbubble Contrast Agent with Focused Ultrasound to Create Brain Lesions at Low Power Levels: MR Imaging and Histologic Study in Rabbits. Radiol 2006;241:95–106.

Mebust WK, Holtgrewe HL, Cockett AT, Peters PC. Transurethral prostatectomy: immediate and postoperative complications. A cooperative study of 13 participating institutions evaluating 3,885 patients. JUrol 1989;141:243–247. [PubMed: 2643719]

Miller D Overview of experimental studies of biological effects of medical ultrasound caused by gas body activation and inertial cavitation. Prog Biophy Mol Biol 2007;93:314–330.

Author Manuscript Author Manuscript Author Manuscript Author Manuscript

Miller DL, Gies RA. The influence of ultrasound frequency and gas-body composition on the contrast agent-mediated enhancement of vascular bioeffects in mouse intestine. Ultrasound Med Biol 2000;26:307–313. [PubMed: 10722920]

Miller RM, Zhang X, Maxwell AD, Cain CA, Xu Z. Bubble-Induced Color Doppler Feedback for Histotripsy Tissue Fractionation. IEEE Trans Ultrason, Ferroelect, Freq Contr 2016;63:408–419.

Movahed P, Kreider W, Maxwell AD, Dunmire B, Freund JB. Ultrasound-Induced Bubble Clusters in Tissue-Mimicking Agar Phantoms. Ultrasound Med Biol 2017;43:2318–2328. [PubMed: 28739379]

Movahed P, Kreider W, Maxwell AD, Hutchens SB, Freund JB. Cavitation-induced damage of soft materials by focused ultrasound bursts: A fracture-based bubble dynamics model. J Acoust Soc Am 2016;140:1374–1386. [PubMed: 27586763]

Myers R, Coviello C, Erbs P, Foloppe J, Rowe C, Kwan J, Crake C, Finn S, Jackson E, Balloul J-M, Story C, Coussios C, Carlisle R. Polymeric Cups for Cavitation-mediated Delivery of Oncolytic Vaccinia Virus. J Am Soc Gene Cell Ther 2016;24:1627–1633.

Ni Y, Mulier S, Miao Y, Michel L, Marchal G. A review of the general aspects of radiofrequency ablation. Abd Imag 2005;30:381–400.

O' Brien WD Jr, Dunn F. An early history of high-intensity focused ultrasound. Physics Today 2015;68:40–45.

O'Reilly MA, Hynynen K. Blood-Brain Barrier: Real-time Feedback-controlled Focused Ultrasound Disruption by Using an Acoustic Emissions-based Controller. Radiol 2012;263:96–106.

Okubo M, Minami H, Morikawa K. Production of micron-sized, monodisperse, transformable rugby-ball-like-shaped polymer particles. Coll Poly Sci 2001;279:931–935.

Oto A, Sethi I, Karczmar G, McNichols R, Ivancevic MK. MR imaging–guided focal laser ablation for prostate cancer: phase I trial. Radiol 2013;267:932–940.

Owens GE, Miller RM, Ensing G, Ives K, Gordon D, Ludomirsky A, Xu Z. Therapeutic ultrasound to noninvasively create intracardiac communications in an intact animal model. Cathet Cardiovasc Intervent 2010;77:580–588.

Pahk KJ, Dhar DK, Malago M, Saffari N. Ultrasonic histotripsy for tissue therapy. J Phys Conf Ser 2015;581:012001.

Pahk KJ, Gélat P, Sinden D, Dhar DK, Saffari N. Numerical and Experimental Study of Mechanisms Involved in Boiling Histotripsy. Ultrasound Med Biol 2017;43:2848–2861. [PubMed: 28965719]

Palmeri ML, Nightingale KR. Acoustic radiation force-based elasticity imaging methods. Interface Focus 2011;1:553–564. [PubMed: 22419986]

Parsons JE, Cain CA, Abrams GD, Fowlkes JB. Pulsed cavitational ultrasound therapy for controlled tissue homogenization. Ultrasound Med Biol 2006;32:115–129. [PubMed: 16364803]

Pierce AD. Acoustics. 3rd ed. Melville: Acoustical Society of America, 1989.

Pishchalnikov YA, Sapozhnikov OA, Bailey MR, Pishchalnikova IV, Williams JC Jr, McAteer JA. Cavitation selectively reduces the negative-pressure phase of lithotripter shock pulses. Acoust Res Lett On 2005;6:280–286.

Prieur F, Zorgani A, Catheline S, Souchon R, Mestas J-L, Lafond M, Lafon C. Observation of a cavitation cloud in tissue using correlation between ultrafast ultrasound images. IEEE Trans Ultrason, Ferroelect, Freq Contr 2015;62:1256–1264.

Prosperetti A, Lezzi A. Bubble dynamics in a compressible liquid. J Fluid Mechanics 1986;168:457–457478.

Radhakrishnan K, Holland CK, Haworth KJ. Scavenging dissolved oxygen via acoustic droplet vaporization. Ultrasonics - Sonochemistry 2016;31:394–403. [PubMed: 26964964]

Rich KT, Mast TD. Methods to calibrate the absolute receive sensitivity of single-element, focused transducers. J Acoust Soc Am 2015a;138:EL193–EL198. [PubMed: 26428812]

Rich KT, Mast TD. Accuracy of a bistatic scattering substitution technique for calibration of focused receivers. J Acoust Soc Am 2015b;138:EL469–EL473. [PubMed: 26627816]

Rieke V, Butts Pauly K. MR thermometry. J Magn Reson Imaging 2008;27:376–390. [PubMed: 18219673]

Author Manuscript Author Manuscript Author Manuscript Author Manuscript

Roberts WW, Hall TL, Duryea AP, Cain CA. Removal of residual cavitation nuclei to enhance histotripsy erosion of model urinary stones. IEEE Trans Ultrason, Ferroelect, Freq Contr 2015;62:896–904.

Roberts WW, Hall TL, Ives K, Wolf JS Jr, Fowlkes JB, Cain CA. Pulsed Cavitational Ultrasound: A Noninvasive Technology for Controlled Tissue Ablation (Histotripsy) in the Rabbit Kidney. J Urol 2006;175:734–738. [PubMed: 16407041]

Rosnitskiy PB, Yuldashev PV, Sapozhnikov OA, Maxwell AD, Kreider W, Bailey MR, Khokhlova VA. Design of HIFU Transducers for Generating Specified Nonlinear Ultrasound Fields. IEEE Trans Ultrason, Ferroelect, Freq Contr 2017;64:374–390.

Roy RA, Madanshetty SI, Apfel RE. An acoustic backscattering technique for the detection of transient cavitation produced by microsecond pulses of ultrasound. J Acoust Soc Am 1990; 87:2451. [PubMed: 2373791]

Salgaonkar VA, Datta S, Holland CK, Mast TD. Passive cavitation imaging with ultrasound arrays. J Acoust Soc Am 2009;126:3071. [PubMed: 20000921]

Sankin GN. Cavitation under spherical focusing of acoustic pulses. Acoust Phys 2006;52:93–103.

Sapozhnikov OA, Bailey MR, Crum LA, Miller NA, Cleveland RO, Pishchalnikov YA, Pishchalnikov IV, McAteer JA, Connors BA, Blomgren PM, Evan AP. Ultrasound-guided localized detection of cavitation during, lithotripsy in pig kidney in vivo. Ultrasonics 2001; 2:1347–1350.

Sboros V, Pye SD, MacDonald CA, Gomatam J, Moran CM, McDicken WN. Absolute measurement of ultrasonic backscatter from single microbubbles. Ultrasound Med Biol 2005;31:1063–1072. [PubMed: 16085097]

Schade GR, Wang Y-N, D'Andrea S, Hwang JH, Lin DW, Bailey MR, Khokhlova TD. Boiling histotripsy ablation of in vivo renal carcinoma in the eker rat. J Urol 2015;193:e459–e460.

Schuster TG, Wei JT, Hendlin K, Jahnke R, Roberts WW. Histotripsy Treatment of Benign Prostatic Enlargement Using the Vortx Rx System: Initial Human Safety and Efficacy Outcomes. Urology 2018; 114:184–187. [PubMed: 29330000]

Shaw GJ, Meunier JM, Huang S-L, Lindsell CJ, McPherson DD, Holland CK. Ultrasound-enhanced thrombolysis with tPA-loaded echogenic liposomes. Thromb Res 2009; 124:306–310. [PubMed: 19217651]

Shpak O, Kokhuis TJA, Luan Y, Lohse D, de Jong N, Fowlkes B, Fabiilli M, Versluis M. Ultrafast dynamics of the acoustic vaporization of phase-change microdroplets. J Acoust Soc Am 2013;134:1610–1621. [PubMed: 23927201]

Simon JC, Sapozhnikov O, Khokhlova V, Wang Y-N, Crum LA, Bailey MR. Ultrasonic atomization of tissue and its role in tissue fractionaction by high intensity focused ultrasound. Phys Med Biol 2012; 57: 8061–8078. [PubMed: 23159812]

Simon JC, Sapozhnikov OA, Kreider W, Breshock M, Williams JCJ, Bailey MR. The role of trapped bubbles in kidney stone detection with the color Doppler ultrasound twinkling artifact. Phys Med Biol 2018;63:025011. [PubMed: 29131810]

Smith DAB, Vaidya SS, Kopechek JA, Huang S-L, Klegerman ME, McPherson DD, Holland CK. Ultrasound-Triggered Release of Recombinant Tissue-Type Plasminogen Activator from Echogenic Liposomes. Ultrasound Med Biol 2010;36:145–157. [PubMed: 19900755]

Smolock AR, Cristescu MM, Vlaisavljevich E, Gendron-Fitzpatrick A, Green C, Cannata J, Ziemlewicz TJ, Lee FT Jr. Robotically Assisted Sonic Therapy as a Noninvasive Nonthermal Ablation Modality: Proof of Concept in a Porcine Liver Model. Radiol 2018;:171544.

Stan CA, Willmott PR, Stone HA, Koglin JE, Liang M, Aquila AL, Robinson JS, Gumerlock KL, Blaj G, Sierra RG, Boutet S, Guillet SAH, Curtis RH, Vetter SL, Loos H, Turner JL, Decker F-J. Negative Pressures and Spallation in Water Drops Subjected to Nanosecond Shock Waves. J Phys Chem Lett 2016;7:2055–2062. [PubMed: 27182751]

Stähr P, Rupprecht HJ, Voigtländer T, Post F, Otto M, Erbel R, Meyer J. A new thrombectomy catheter device (AngioJet) for the disruption of thrombi: An in vitro study. Cathet Cardiovasc Intervent 1999;47:381–389.

Styn NR, Wheat JC, Hall TL, Roberts WW. Histotripsy of VX-2 Tumor Implanted in a Renal Rabbit Model. JEndourol 2010;24:1145–1150. [PubMed: 20575696]

Author Manuscript Author Manuscript Author Manuscript Author Manuscript

Sukovich J, Pandey A, Gerhardson T, Hall T, Cain C, Xu Z. Rapid liquefaction of blood clots using histotripsy in an in vivo porcine intracerebral hemorrhage (ICH) model. 2017 IEEE International Ultrasonics Symposium (IUS) IEEE, 2017 pp. 1–1.

Sukovich JR, Xu Z, Kim Y, Cao H, Nguyen T-S, Pandey AS, Hall TL, Cain CA. Targeted Lesion Generation Through the Skull Without Aberration Correction Using Histotripsy. IEEE Trans Ultrason, Ferroelect, Freq Contr 2016;63:671–682.

Sun T, Zhang Y, Power C, Alexander PM, Sutton JT, Aryal M, Vykhodtseva N, Miller EL, McDannold NJ. Closed-loop control of targeted ultrasound drug delivery across the blood–brain/tumor barriers in a rat glioma model. Proc Nat Acad Sci 2017;114:E10281–E10290. [PubMed: 29133392]

Szabo TL. Diagnostic Ultrasound Imaging: Inside Out (Biomedical Engineering). 1st ed Academic Press, 2004.

Tatli S, Acar M, Silverman S. Percutaneous cryoablation: techniques and clinical applications. Diagn Interv Radiol 2009; 16:90–95. [PubMed: 19998248]

Tavakkoli J, Sanghvi NT. “Ultrasound-guided HIFU and thermal ablation” in Therapeutic ultrasound: mechanisms to applications. 1st ed., Frekel V, Ed., New York: Nova Science Publishers, 2011, pp. 137–161.

Tejwani R, Young BJ, Wang H-HS, Wolf S, Purves JT, Wiener JS, Routh JC. Open versus minimally invasive surgical approaches in pediatric urology: Trends in utilization and complications. JPedUrol 2017;13:283.el–283.e9.

Tiukinhoy-Laing SD, Buchanan K, Parikh D, Huang S, MacDonald RC, McPherson DD, Klegerman ME. Fibrin targeting of tissue plasminogen activator-loaded echogenic liposomes. J Drug Targ 2007;15:109–114.

Tran BC, Seo J, Hall TL, Fowlkes JB. Microbubble-enhanced cavitation for noninvasive ultrasound surgery. IEEE Trans Ultrason, Ferroelect, Freq Contr 2003;50:1296–1304.

Turrentine FE, Wang H, Simpson VB, Jones RS. Surgical Risk Factors, Morbidity, and Mortality in Elderly Patients. J Am College Surg 2006;203:865–877.

Vlaisavljevich E, Aydin O, Durmaz YY, Lin K-W, Fowlkes B, ElSayed M, Xu Z. Effects of ultrasound frequency on nanodroplet-mediated histotripsy. Ultrasound Med Biol 2015a;41:2135–2147. [PubMed: 25959056]

Vlaisavljevich E, Aydin O, Durmaz YY, Lin K-W, Fowlkes B, Xu Z, ElSayed MEET Effects of Droplet Composition on Nanodroplet-Mediated Histotripsy. Ultrasound Med Biol 2016a;42:931–946. [PubMed: 26774470]

Vlaisavljevich E, Aydin O, Lin K-W, Yuksel Durmaz Y, Fowlkes B, ElSayed M, Xu Z. The role of positive and negative pressure on cavitation nucleation in nanodroplet-mediated histotripsy. Phys Med Biol 2016b;61:663. [PubMed: 26716568]

Vlaisavljevich E, Durmaz YY, Maxwell A, ElSayed M, Xu Z. Nanodroplet-Mediated Histotripsy for Image-guided Targeted Ultrasound Cell Ablation. Theran 2013a ;3:851–864.

Vlaisavljevich E, Gerhardson T, Hall T, Xu Z. Effects of f-number on the histotripsy intrinsic threshold and cavitation bubble cloud behavior. Phys Med Biol 2017a;62:1269–1290. [PubMed: 27995900]

Vlaisavljevich E, Greve J, Cheng X, Ives K, Shi J, Jin L, Arvidson A, Hall T, Welling TH, Owens G, Roberts W, Xu Z. Non-Invasive Ultrasound Liver Ablation Using Histotripsy: Chronic Study in an In Vivo Rodent Model. Ultrasound Med Biol 2016c;42:1890–1902. [PubMed: 27140521]

Vlaisavljevich E, Kim Y, Allen S, Owens G, Pelletier S, Cain C, Ives K, Xu Z. Image-guided non-invasive ultrasound liver ablation using histotripsy. Ultrasound Med Biol 2013b;39:1398–1409. [PubMed: 23683406]

Vlaisavljevich E, Kim Y, Allen S, Owens G, Pelletier S, Cain C, Ives K, Xu Z. Image-Guided Non-invasive Ultrasound Liver Ablation Using Histotripsy: Feasibility Study in an In Vivo Porcine Model. Ultrasound Med Biol 2013c;39:1398–1409. [PubMed: 23683406]

Vlaisavljevich E, Lin K-W, Maxwell A, Warnez MT, Mancia L, Singh R, Putnam AJ, Fowlkes B, Johnsen E, Cain C, Xu Z. Effects of ultrasound frequency and tissue stiffness on the histotripsy intrinsic threshold for cavitation. Ultrasound Med Biol 2015b;41:1651–1667. [PubMed: 25766571]

Author Manuscript Author Manuscript Author Manuscript Author Manuscript

Vlaisavljevich E, Lin K-W, Warnez MT, Singh R, Mancia L, Putnam AJ, Johnsen E, Cain C, Xu Z. Effects of tissue stiffness, ultrasound frequency, and pressure on histotripsy- induced cavitation bubble behavior. Phys Med Biol 2015c;:2271–2292. [PubMed: 25715732]

Vlaisavljevich E, Maxwell A, Mancia L, Johnsen E, Cain C, Xu Z. Visualizing the Histotripsy Process: Bubble Cloud-Cancer Cell Interactions in a Tissue-Mimicking Environment. Ultrasound Med Biol 2016d;42:2466–2477. [PubMed: 27401956]

Vlaisavljevich E, Maxwell A, Warnez M, Johnsen E, Cain CA, Xu Z. Histotripsy-induced cavitation cloud initiation thresholds in tissues of different mechanical properties. IEEE Trans Ultrason, Ferroelect, Freq Contr 2014;61:341–352.

Vlaisavljevich E, Owens G, Lundt J, Teofilovic D, Ives K, Duryea A, Bertolina J, Welling TH, Xu Z. Non-invasive Liver Ablation Using Histotripsy: Preclinical Safety Study in an In Vivo Porcine Model. Ultrasound Med Biol 2017b;43:1237–1251. [PubMed: 28318889]

Vlaisavljevich E, Xu Z, Arvidson A, Jin L, Roberts W, Cain C. Effects of Thermal Preconditioning on Tissue Susceptibility to Histotripsy. Ultrasound Med Biol 2015d;41:2938–2954. [PubMed: 26318560]

Vlaisavljevich E, Xu Z, Maxwell AD, Mancia L, Zhang X, Lin K-W, Duryea AP, Sukovich JR, Hall TL, Johnsen E, Cain CA. Effects of Temperature on the Histotripsy Intrinsic Threshold for Cavitation. IEEE Trans Ultrason, Ferroelect, Freq Contr 2016e;63:1064–1077.

Wang T-Y, Hall TL, Xu Z, Fowlkes JB, Cain CA. Imaging feedback for histotripsy by characterizing dynamics of acoustic radiation force impulse (ARFI)-induced shear waves excited in a treated volume. IEEE Trans Ultrason, Ferroelect, Freq Contr 2014;61:1137–1151.

Wang T-Y, Xu Z, Hall TL, Fowlkes JB, Cain CA. An Efficient Treatment Strategy for Histotripsy by Removing Cavitation Memory. Ultrasound Med Biol 2012;38:753–766. [PubMed: 22402025]

Wang YC, Brennen CE. Numerical computation of shock waves in a spherical cloud of cavitation bubbles. J Fluid Eng 1999;121:872–880.

Xu Z, Fowlkes JB, Cain CA. A new strategy to enhance cavitational tissue erosion using a high-intensity, initiating sequence. IEEE Trans Ultrason, Ferroelect, Freq Contr 2006a;53:1412–1424.

Xu Z, Fowlkes JB, Cain CA. A new strategy to enhance cavitational tissue erosion using a high-intensity, initiating sequence. IEEE Trans Ultrason, Ferroelect, Freq Contr IEEE, 2006b; 53:1412–1424.

Xu Z, Fowlkes JB, Rothman ED, Levin AM, Cain CA. Controlled ultrasound tissue erosion: The role of dynamic interaction between insonation and microbubble activity. The Journal of the acoustical Society of America 2005;117:424. [PubMed: 15704435]

Xu Z, Hall TL, Fowlkes JB, Cain CA. Optical and acoustic monitoring of bubble cloud dynamics at a tissue-fluid interface in ultrasound tissue erosion. J Acoust Soc Am 2007a;121:2421. [PubMed: 17471753]

Xu Z, Hall TL, Fowlkes JB, Cain CA. Optical and acoustic monitoring of bubble cloud dynamics at a tissue-fluid interface in ultrasound tissue erosion. J Acoust Soc Am 2007b;121:2421–10. [PubMed: 17471753]

Xu Z, Ludomirsky A, Eun LY, Hall TL, Tran BC, Fowlkes JB, Cain CA. Controlled ultrasound tissue erosion. IEEE Trans Ultrason, Ferroelect, Freq Contr IEEE, 2004;51:726–736.

Xu Z, Owens G, Gordon D, Cain C, Ludomirsky A. Noninvasive Creation of an Atrial Septal Defect by Histotripsy in a Canine Model. Circul 2010;121:742–749.

Xu Z, Roberts WW, Hall TL, Duryea AP, Maxwell AD, Cain CA. In vitro comminution of model renal calculi using histotripsy. IEEE Trans Ultrason, Ferroelect, Freq Contr 2011;58:971–980.

Yand B, Prosperetti A. Vapour bubble collapse in isothermal and non-isothermal liquids. J Fluid Mechn 2008;601:253–279.

Yang X, Church CC. A model for the dynamics of gas bubbles in soft tissue. J Acoust Soc Am 2005;118:3595. [PubMed: 16419805]

Yoshizawa S, Takagi R, Yasuda J, Umemura S-I. Enhancement of cavitation inception by second-harmonic superimposition. AГР Conf Proc 2012; 1474: 235–238.

Yuksel Durmaz Y, Vlaisavljevich E, Xu Z, ElSayed M. Development of Nanodroplets for Histotripsy-Mediated Cell Ablation. Mol Pharmaceutics 2014;11:3684–3695.

Author Manuscript Author Manuscript Author Manuscript Author Manuscript

Zhang X, Macoskey JJ, Ives K, Owens GE, Gurm HS, Shi J, Pizzuto M, Cain CA, Xu Z. Non-Invasive Thrombolysis Using Microtripsy in a Porcine Deep Vein Thrombosis Model. Ultrasound Med Biol 2017;43:1378–1390. [PubMed: 28457630]

Zhang X, Miller RM, Lin K-W, Levin AM, Owens GE, Gurm HS, Cain CA, Xu Z. Real-time feedback of histotripsy thrombolysis using bubble-induced color Doppler. Ultrasound Med Biol 2015;41:1386–1401. [PubMed: 25623821]

Xu Zhen, Raghavan M Hall TL, Mycek MA Fowlkes JB, Cain CA. Evolution of bubble clouds induced by pulsed cavitational ultrasound therapy - Histotripsy. IEEE Trans Ultrason, Ferroelect, Freq Contr 55:1122–1132.

Zheng Q, Durben DJ, Wolf GH, Angell CA. Liquids at Large Negative Pressures: Water at the Homogeneous Nucleation Limit. Sci Am Assoc Ad Sci 1991;254:829–832.

Zhong P, Cioanta I, Cocks FH. Inertial cavitation and associated acoustic emission produced during electrohydraulic shock wave lithotripsy. J Acoust Soc Am 1997;101:2940–2950. [PubMed: 9165740]

Zhou Y-F. High intensity focused ultrasound in clinical tumor ablation. Wor J Clin Oncol 2011;2:8–20.

Author Manuscript Author Manuscript Author Manuscript Author Manuscript

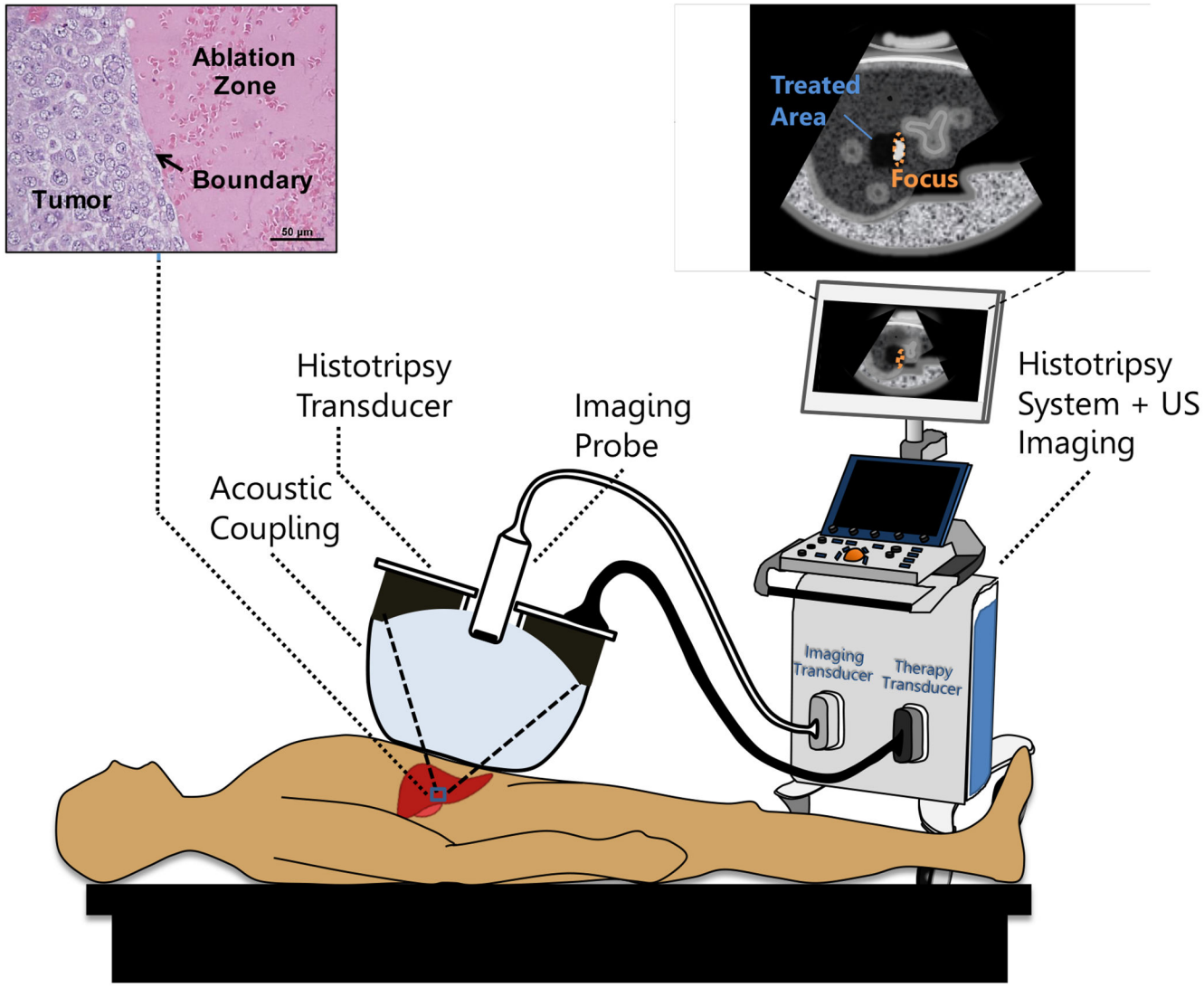

Fig. 1:

Conceptual illustration of a noninvasive histotripsy procedure. A focused ultrasound transducer is coupled to the patient through a confined water bolus attached to the transducer face. The transducer also contains an ultrasound (US) imaging probe for targeting and guidance. Both transducers are controlled by a combined imaging/therapy system. The transducer focus is positioned within the target tissue using US imaging guidance. When therapy is administered, bubbles appear on the US image as a hyperechoic region confined to the focus. Over a short time, the tissue is disintegrated into subcellular debris with a precise boundary. Once the tissue is ablated, it appears on imaging as a hypoechoic area indicating to the operator that treatment is complete.

Author Manuscript Author Manuscript Author Manuscript Author Manuscript

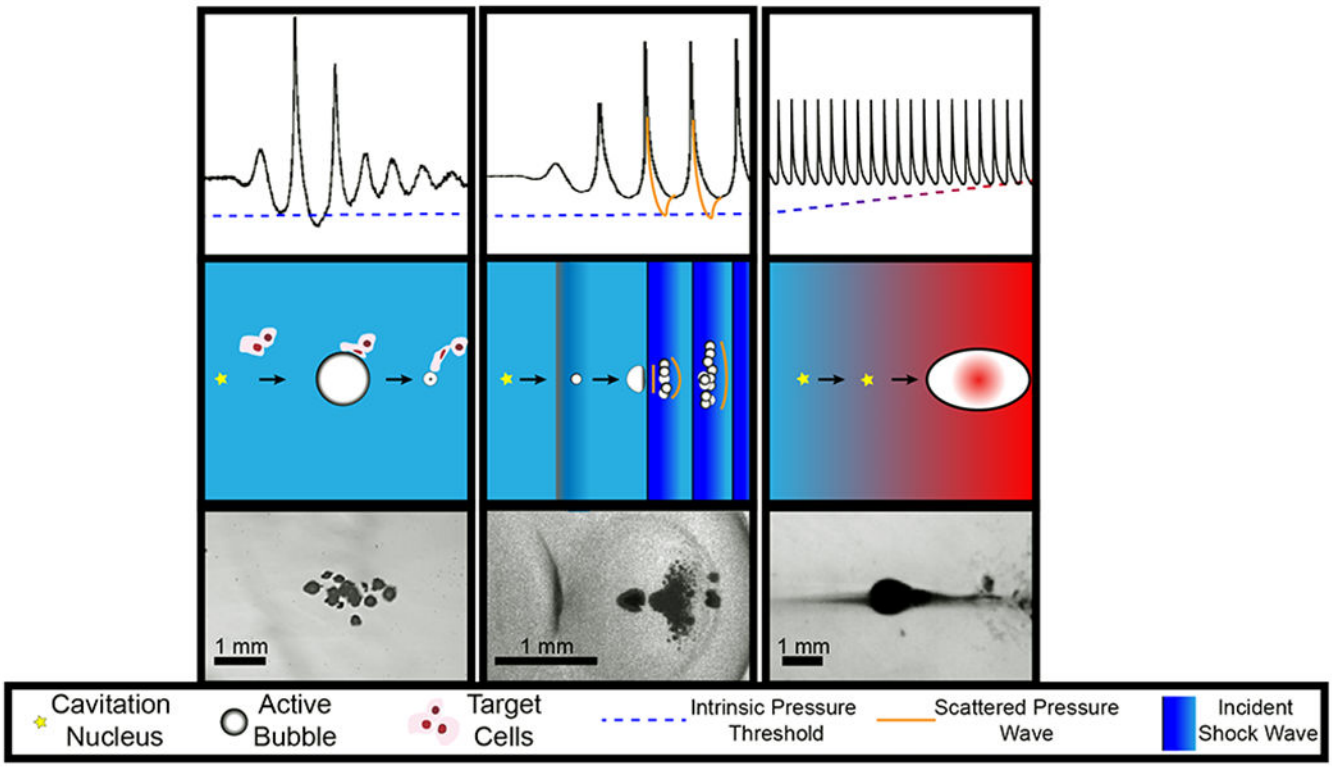

Fig. 2:

Summary of histotripsy-induced cavitation dynamics. For all forms of histotripsy, nanoscale nuclei intrinsic to the medium are present in the tissue. **Left Column:** For intrinsic threshold insonations, the cavitation nucleus is activated with a single-cycle pulse with tension below the intrinsic medium threshold (left arrow, middle row). The expanded bubble then undergoes an inertial collapse under ambient pressure (right arrow, middle row). **Middle Column:** In shock-scattering histotripsy excitations, the activated nucleus grows slowly over the course of several cycles (left arrow, middle row) and deforms due to the incident shock waves (right arrow, middle row). Additional bubbles form spatially and temporally in regions of constructive interference between the incident wave, and waves scattered by the deformed bubble. **Right column:** In boiling histotripsy, shock-enhanced heating alters cavitation nucleus (left arrow, middle tow) to reduce the requisite tension for bubble formation (right arrow, middle row). For all forms of histotripsy, the expansion and contraction of the bubble imparts lethal strain on the cellular and extracellular components of the tissue in close proximity to the bubble (depicted in left column, middle row only). Representative frames from high speed videography of histotripsy-generated bubbles are shown in the bottom row. Note: Bubble sizes and nuclei in second row not to scale.

Author Manuscript Author Manuscript Author Manuscript Author Manuscript

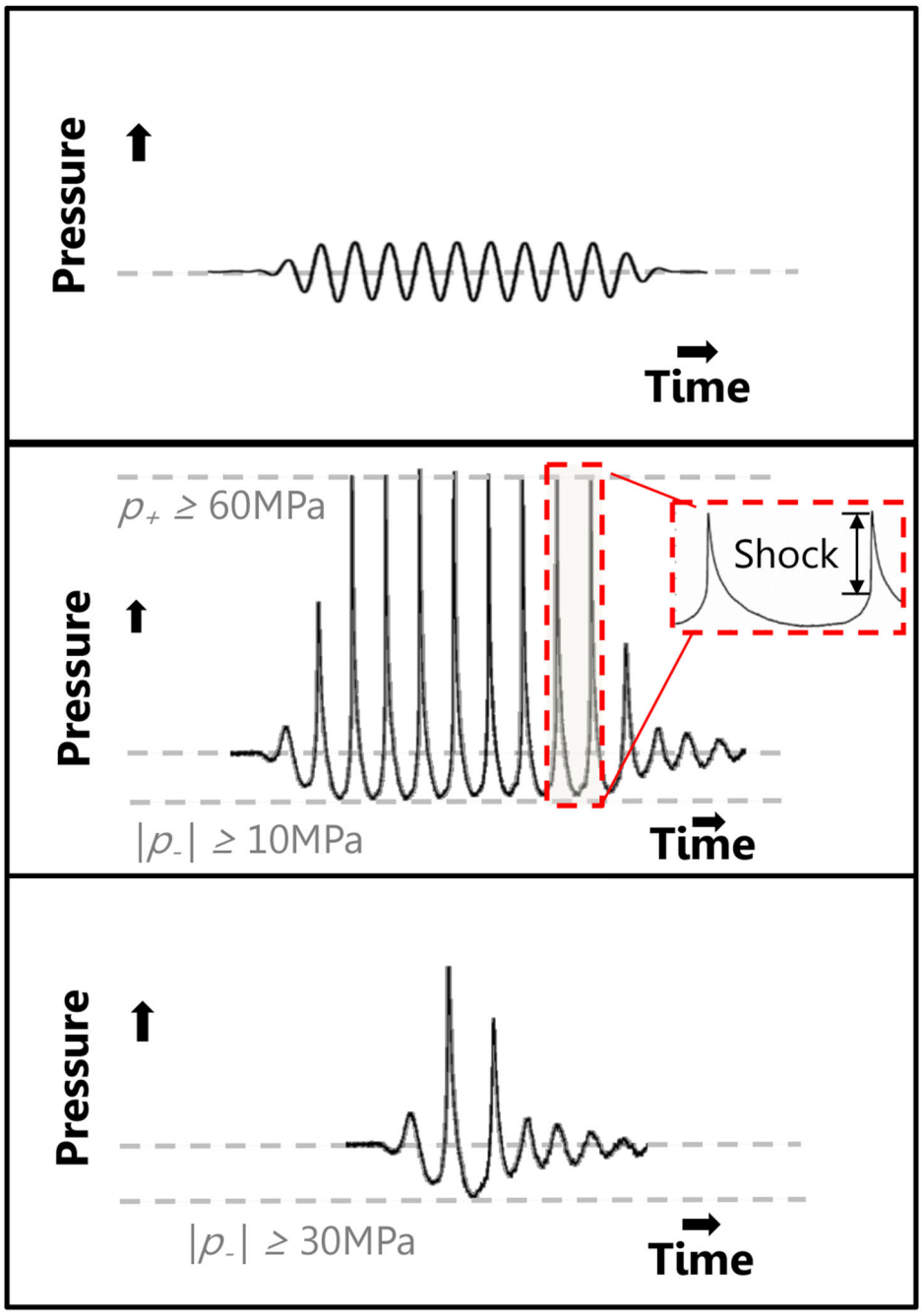

Fig. 3:

Focal pressure waveforms generated by a source in the linear (top panel) and nonlinear (bottom panel) regime with a 10-cycle pulse. A short pulse, such as that used in intrinsic-threshold histotripsy is shown in the middle panel. Note the highly asymmetric waveform in the middle and bottom panels, typical for focused sources due to the combined effects of diffraction and nonlinear propagation.

Author Manuscript Author Manuscript Author Manuscript Author Manuscript

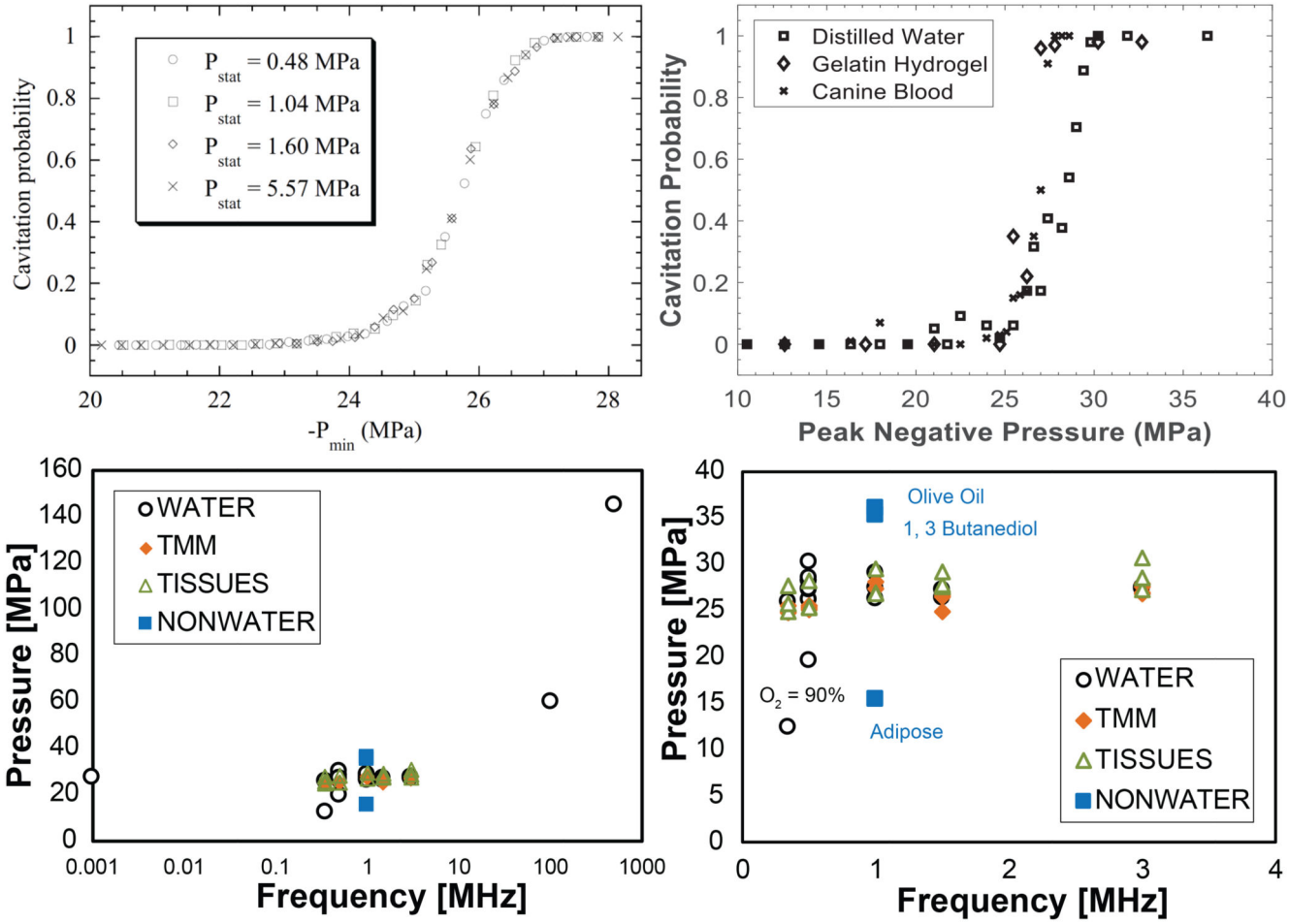

Fig. 4:

Cavitation probability vs. pulse peak negative pressure measured by Herbert et al. (2006) in water under different hydrostatic pressures (Top Left) and in several media by Maxwell et al. 2013 at 1 MHz (Top Right). These and other measurements suggest the probability for histotripsy-induced cavitation is greater than 0.5 for peak negative pressures greater than 26-30 MPa. (Bottom Left) Pressure in MPa to achieve a 50% cavitation probability or the minimum pressure required to initiate cavitation detectable via acoustic backscatter (P_{min}) for different materials (Maxwell et al. 2013; Vlaisavljevich et al. 2015b). (Bottom Right) The same plot focused on frequencies of interest for most histotripsy applications. *Top left panel is reprinted from Physical Review E, vol. 74, Herbert et al, Cavitation pressure in water, p. 041603 1-22, Copyright (2006), with permission from the American Physical Society.*

Author Manuscript Author Manuscript Author Manuscript Author Manuscript

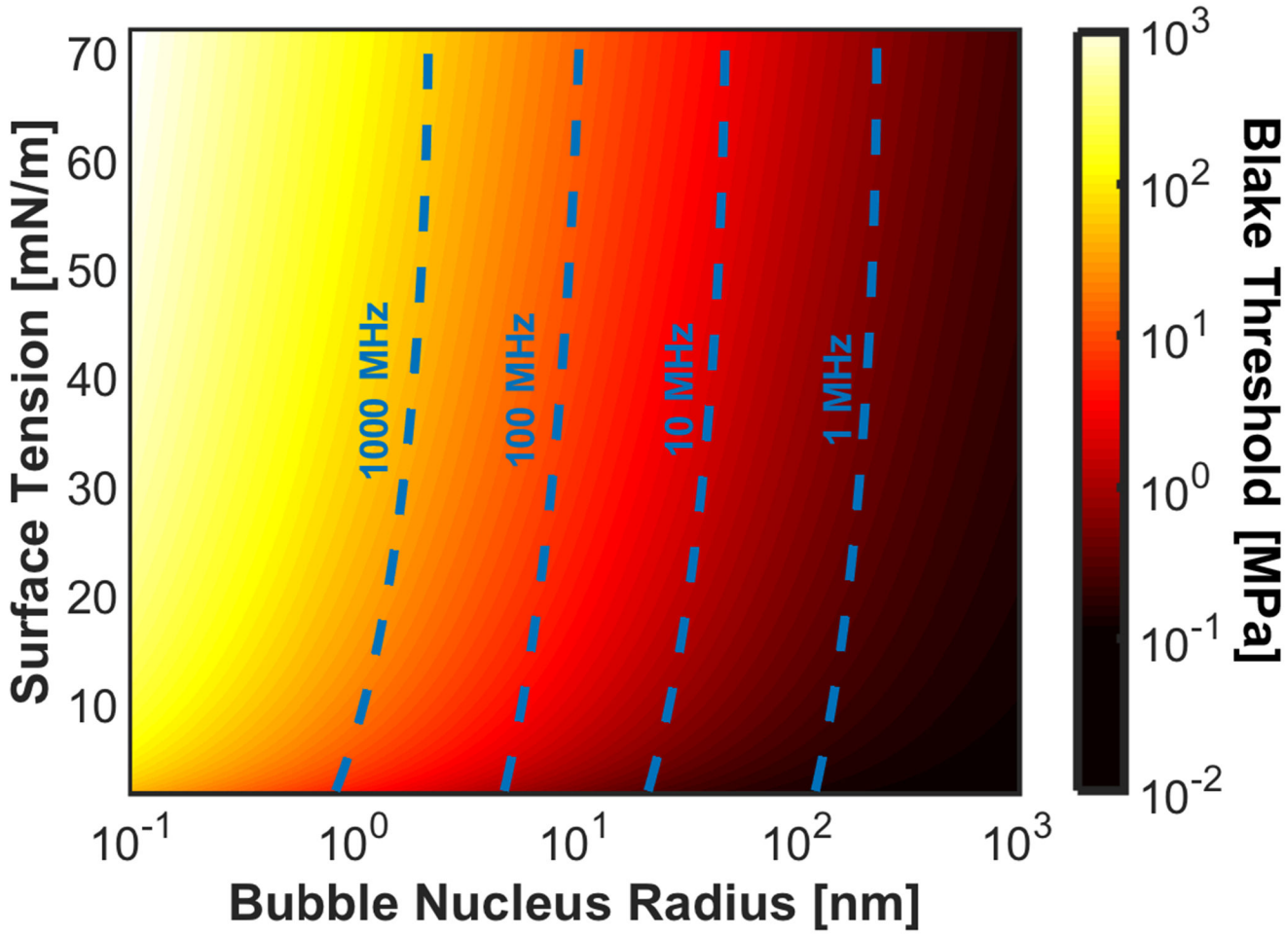

Fig. 5:

Blake threshold as a function of bubble nucleus radius and surface tension. The resonant frequency, calculated in the absence of viscosity and elasticity, of the bubble nuclei are noted in the dashed, blue lines.

Author Manuscript Author Manuscript Author Manuscript Author Manuscript

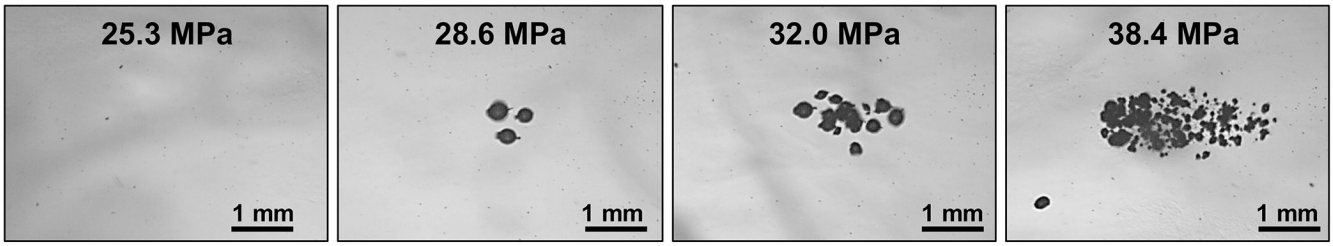

Fig. 6:

Bubbles generated by a one cycle histotripsy pulse using a 500 kHz array transducer in an agar phantom as a function of peak negative pressure. *Reprinted from Physics in Medicine and Biology, vol. 62, Vlaisavljevich et al, Effects of f-number on the histotripsy intrinsic threshold and cavitation bubble cloud behavior, p. 1269, Copyright (2017),* doi.org/10.1088/1361-6560/aa54c7. *© Institute of Physics and Engineering in Medicine. Reproduced by permission of IOP Publishing. All rights reserved.*

Author Manuscript Author Manuscript Author Manuscript Author Manuscript

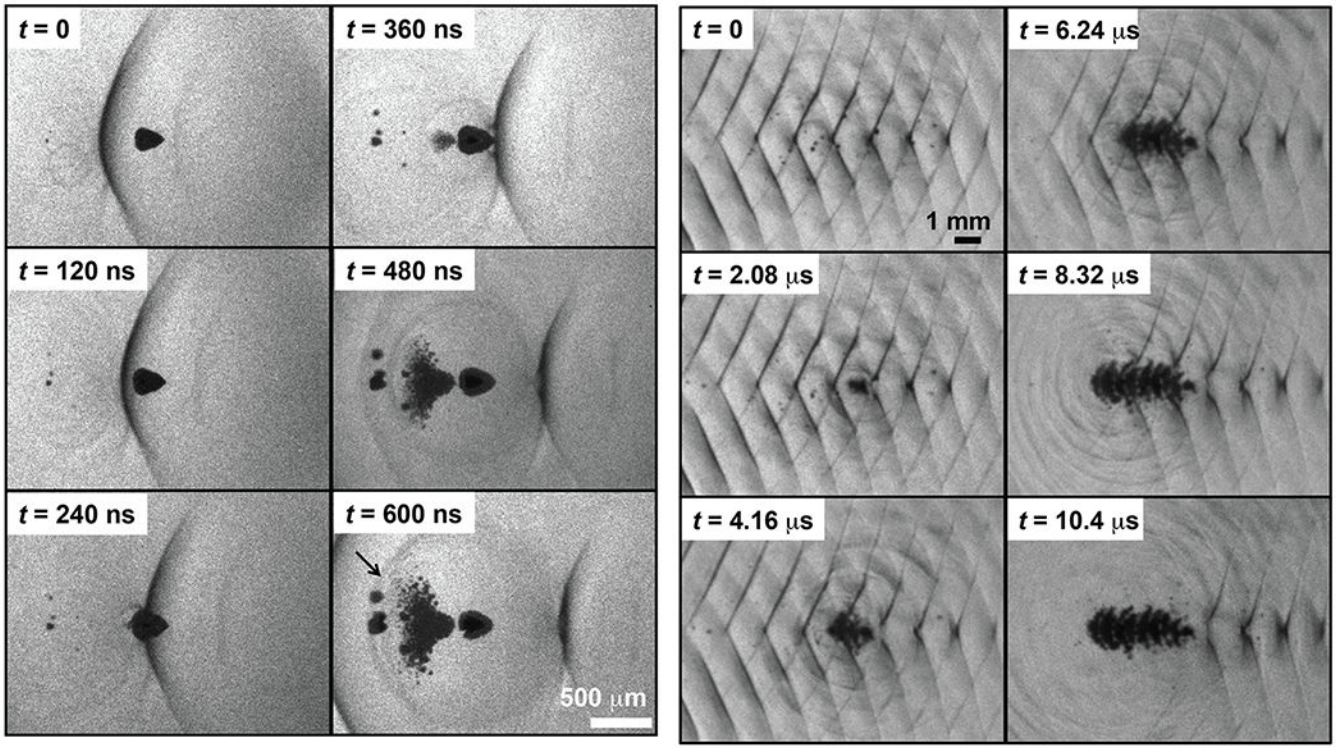

Fig. 7:

(Left) Initiation of a bubble cloud via shock scattering captured by shadowography. Ultrasound propagation is from left to right. The scattering bubble (dark cone, $t = 0$ frame) has been distorted due to the asymmetric incident shock wave (dark line). The large size of the scattering bubble compared to the shock thickness and the flattened surface allow strong scattering of the incident shock wave. Furthermore, the pressure release boundary condition of the bubble/gel interface invert the shock. The scattered, inverted wave nucleate cavitation proximal to the bubble. (Right) A shadowgraph sequence showing formation of a bubble cloud over a 15-cycle pulse. The acoustic propagation is left to right, but cloud growth forms in the opposite direction during passage of the pulse.

Author Manuscript Author Manuscript Author Manuscript Author Manuscript

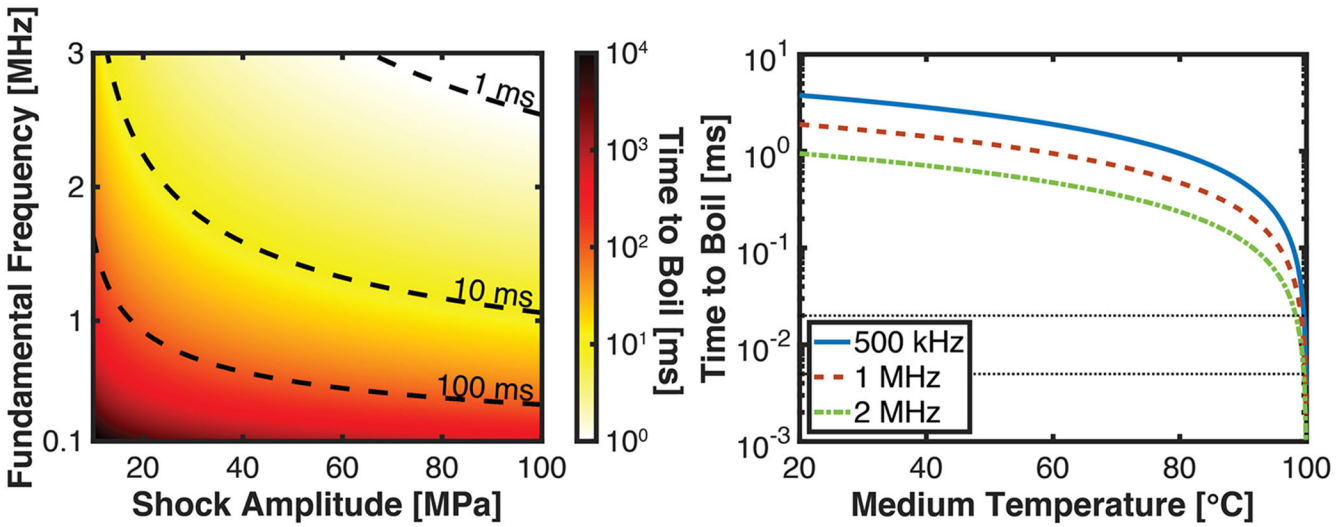

Fig. 8:

(A) Time to boil for shock-induced heating in soft tissues. (B) Time to boil as a function of the temperature of the medium. The center frequency of the insonation is noted in the legend, and a 100 MPa shock amplitude was assumed. The dashed back lines span 5-20 μs in panels B, the typical duration of a shock scattering histotripsy pulse (Khokhlova et al. 2015; Maxwell et al. 2012). The specific heat per unit mass was 3.5×10^6 J/m^3•C.

Author Manuscript Author Manuscript Author Manuscript Author Manuscript

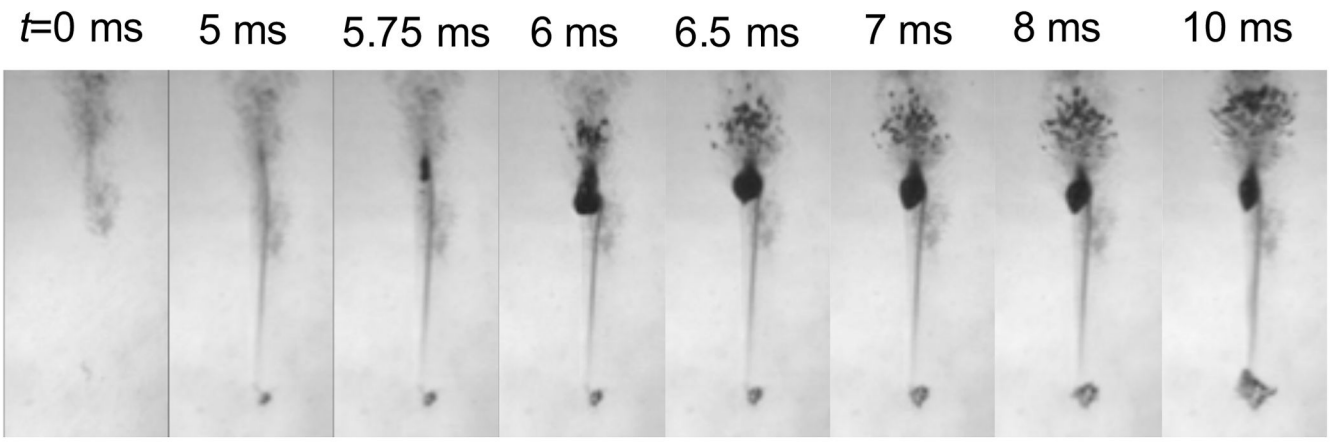

Fig. 9:

Temporal sequence of millisecond boiling at the focus of a 1-MHz boiling histotripsy transducer. As heat is deposited, a shadow appears due to changes in index of refraction around the focus ($t = 5$ ms). At $t = 5.75$ ms, a boiling bubble occurs, and a cavitation cloud appears behind the bubble over the next 0.5 ms due to scattering. Ultrasound propagation is from top to bottom.

Author Manuscript Author Manuscript Author Manuscript Author Manuscript

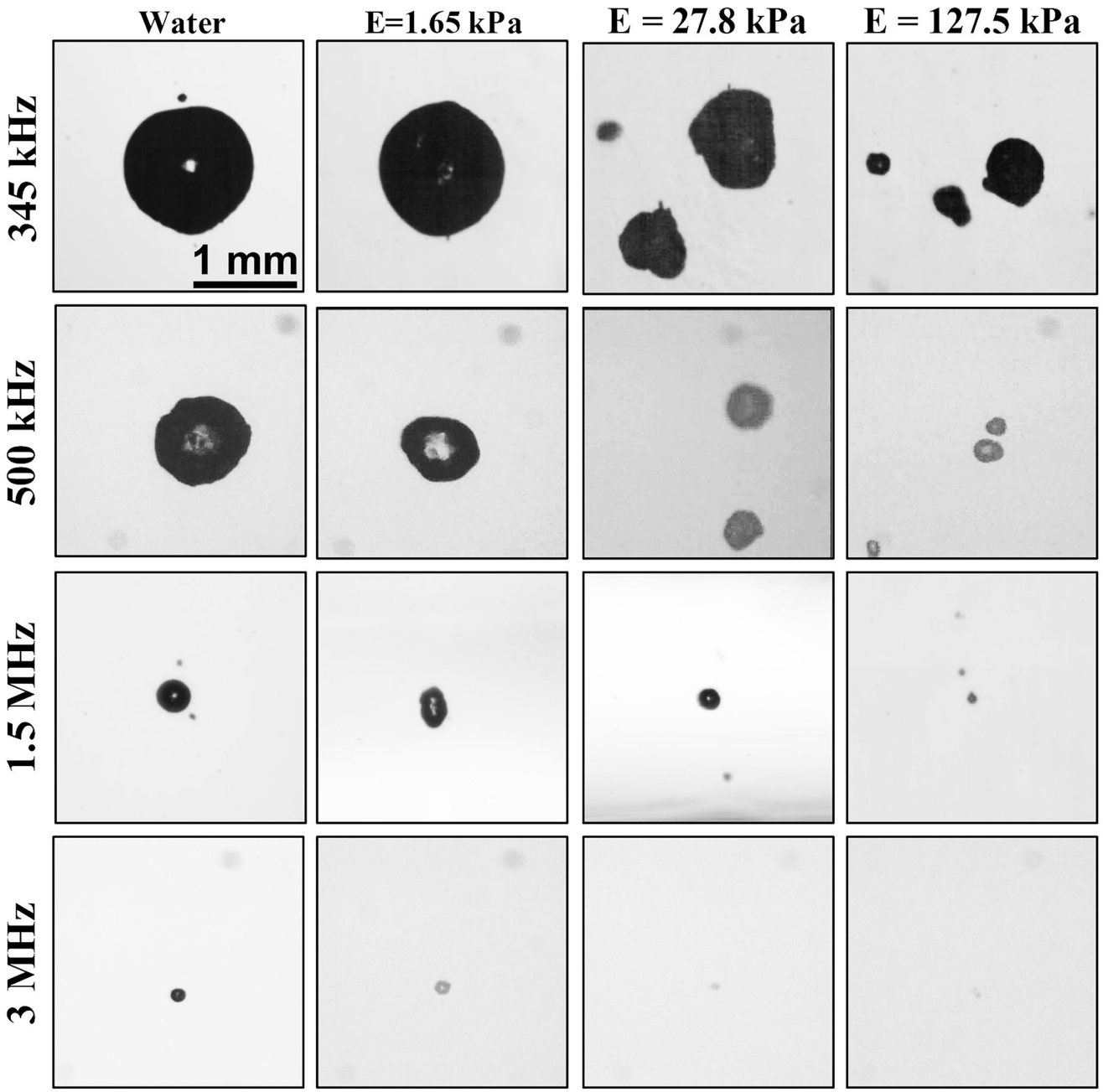

Fig. 10:

Optical images of bubbles produced by histotripsy pulses inside agarose tissue phantoms of increasing Young's modulus. Images demonstrate a decrease in bubble size with increasing frequency and increasing medium stiffness. *Reprinted from Physics in Medicine and Biology, vol. 60, Vlaisavljevich et al, Effects of tissue stiffness, ultrasound frequency, and pressure on histotripsy-induced cavitation bubble behavior, p. 2271,* doi.org/10.1088/0031-9155/60/6/2271. *Copyright (2015), © Institute of Physics and Engineering in Medicine. Reproduced by permission of IOP Publishing. All rights reserved.*

Author Manuscript Author Manuscript Author Manuscript Author Manuscript

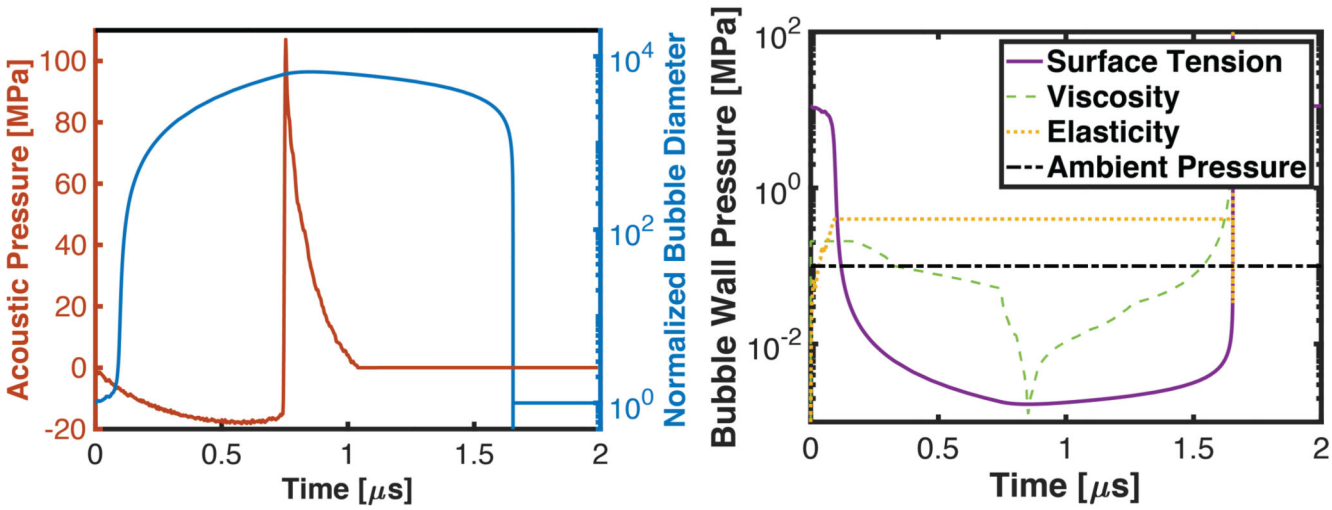

Fig. 11:

Left: Calculated response of a 20-nm diameter bubble (right hand axis) to a single cycle of a shock scattering histotripsy pulse (left hand axis) via the Yang/Church model (Yang and Church 2005). **Right:** External pressure forces acting on bubble wall during the excitation due to surface tension, viscosity, elasticity, and the ambient pressure (0.1 MPa). The following values of the medium properties were used: surface tension, $\sigma = 56$ mN/m, dynamic viscosity, $\mu = 0.005$ kg/m•s, and elastic modulus, $E = 100$ kPa. The exact pressure at the bubble wall will change for variations in the cavitation process (e.g. bubble size, medium properties, histotripsy excitation), though the trends will remain (Bader 2018).

Author Manuscript Author Manuscript Author Manuscript Author Manuscript

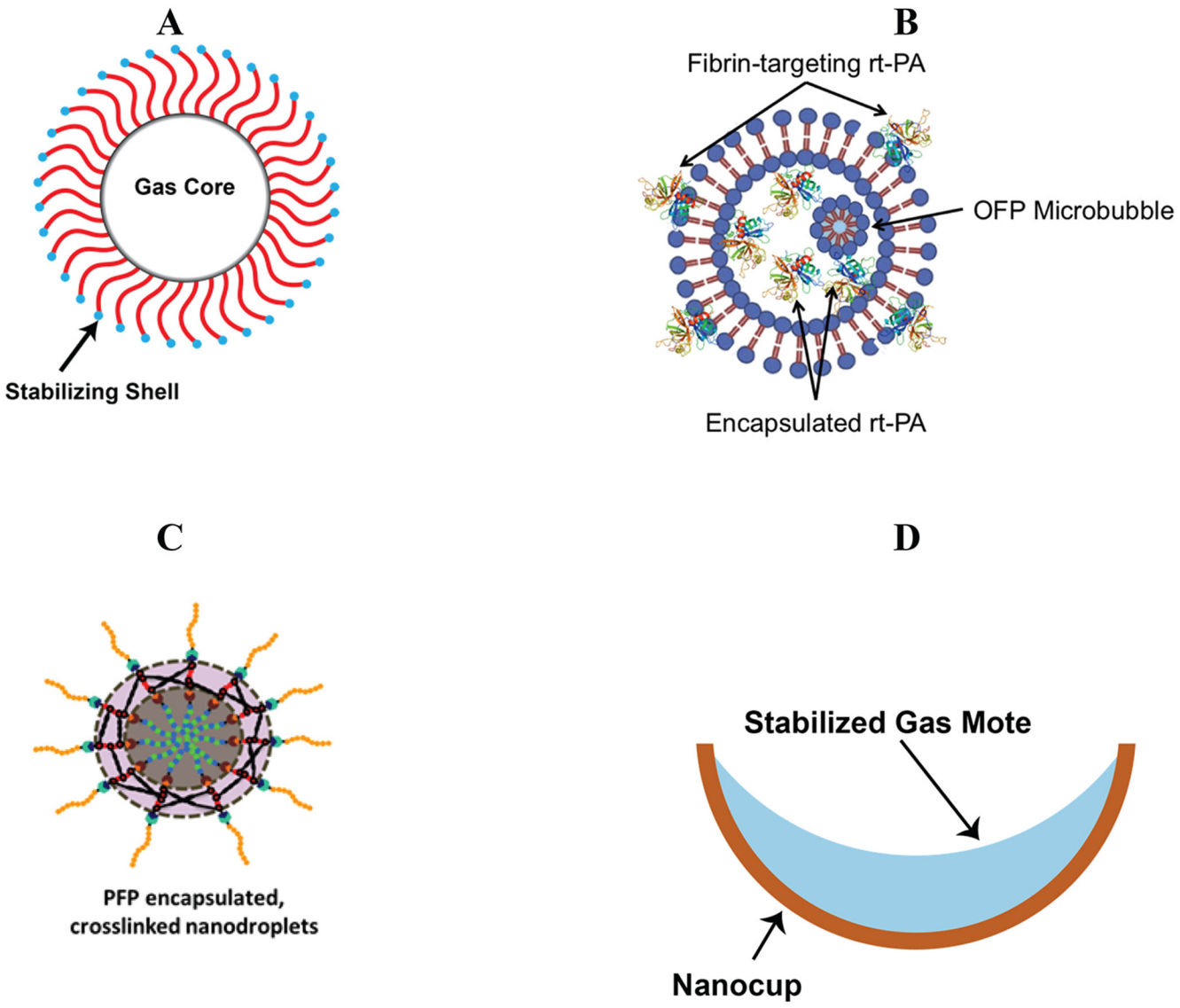

Fig. 12:

Overview of exogenous nuclei utilized in histotripsy. (A) Microbubble contrast agent, typically composed of a high molecular weight gas (e.g. C3F8) surrounded by a stabilizing shell, such as a lipid. (B) Schematic of echogenic liposome loaded with the thrombolytic drug rt-PA and octafluoropropane gas microbubbles. A portion of the thrombolytic is encapsulated within the liposome. The remaining portion is intercalated within the lipid bilayer, exposing the finger domain to target fibrin. Upon exposure to a histotripsy pulse, the encapsulated bubble will expand, locally releasing the thrombolytic. (C) Polymer encapsulated nanodroplets containing perfluorocarbon liquid core used to lower the cavitation nucleation threshold. (D) Nanocup used to entrap and stabilize gas to act as an extrinsic cavitation nucleus.

Author Manuscript Author Manuscript Author Manuscript Author Manuscript

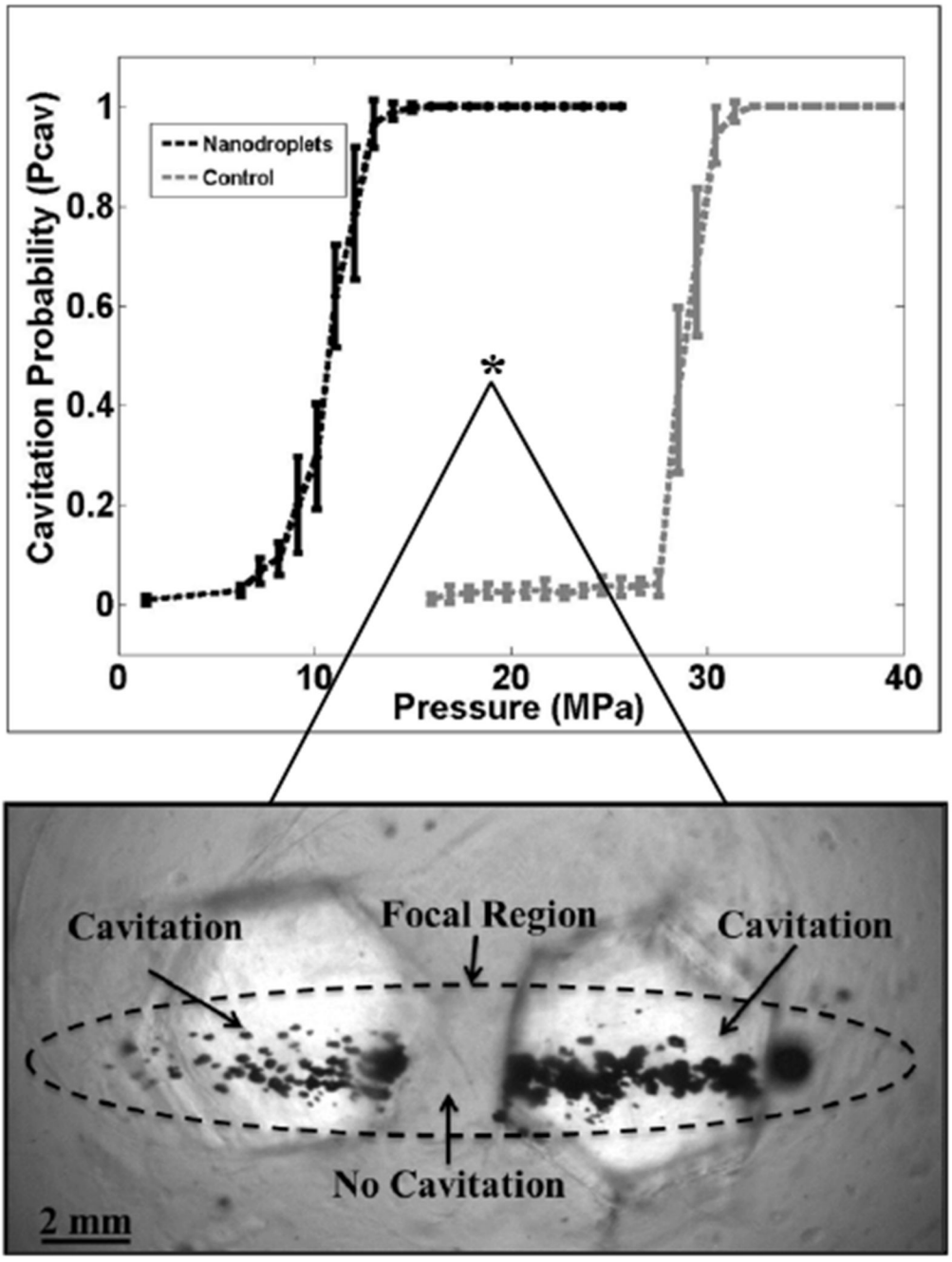

Fig. 13:

Nanodroplet-mediated histotripsy. (A) Perfluorocarbon nanodroplets significantly reduce the histotripsy intrinsic threshold, allowing for (B) selective generation of cavitation only in regions containing the targeted nanodroplets. *Reprinted from Theranostics, vol. 3, Vlaisavljevich et al, Nanodroplet-mediated histotripsy for image-guided targeted ultrasound cell ablation, p. 851,* doi:10.7150/thno.6717.(*2013*).

Author Manuscript Author Manuscript Author Manuscript Author Manuscript

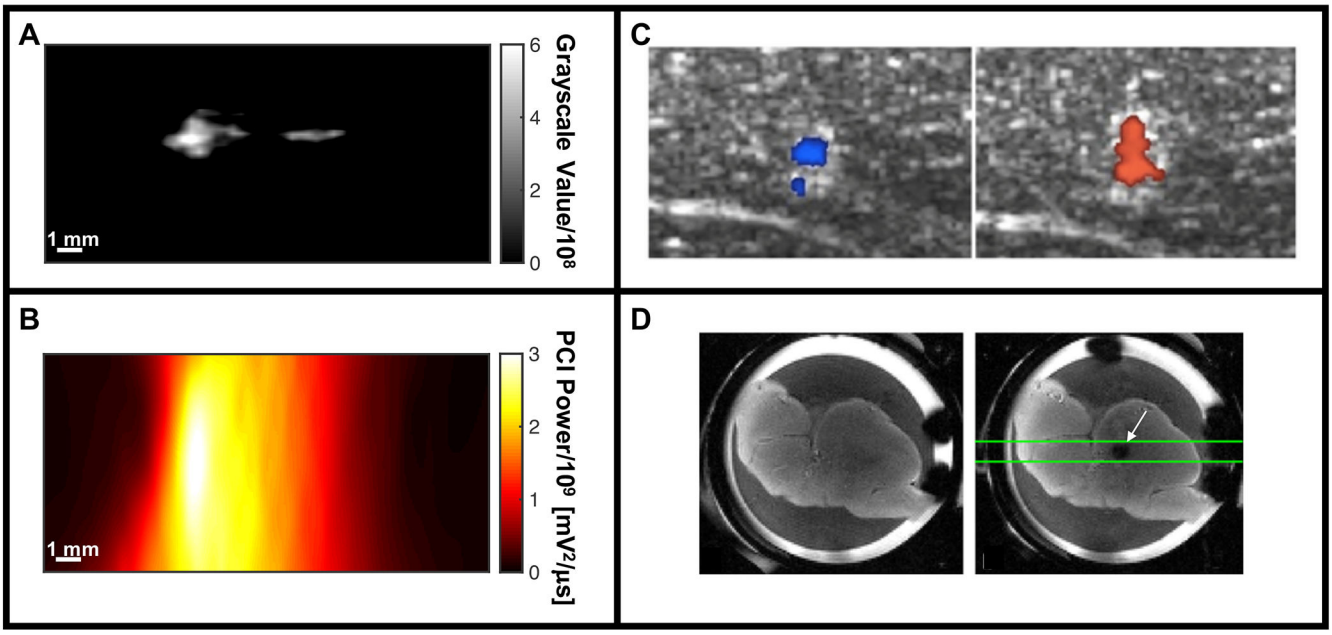

Fig. 14:

Summary of imaging modalities for real-time assessment for histotripsy image guidance. (A) B-mode imaging of hyperechoic bubble cloud via changes in grayscale value (histotripsy pulse propagating from left to right in the image). (B) Passive cavitation imaging (PCI) maps acoustic emissions generated by the bubble cloud spatially (histotripsy pulse propagating from left to right in the image). (C) Color Doppler images acquired during histotripsy liquefaction of *ex vivo* porcine liver, indicating movement both towards (left image) and away from (right image) due to coherent motion associated with translation of the bubble cloud (Miller et al. 2016). (D) *Ex vivo* porcine liver sample prior to histotripsy excitation imaged with a spin-echo imaging sequence (left frame), and just after histotripsy excitation with a cavitation-sensitive 2D EPI sequence (white arrow, right frame) (Allen et al. 2015).

*Panel C reprinted with permission from IEEE Transactions on Ultrasonics, Ferroelectrics and Frequency Control, vol. 63, Miller et al, Bubble-induced color Doppler feedback for histotripsy tissue fractionation, p. 408, doi:*10.1109/TUFFC.2016.2525859. *Copyright (2016), © IEEE. Panel D reprinted with permission from Magnetic Resonance in Medicine, vol. 76, Allen et al, MR-based detection of individual bubble clouds form in tissue and phantoms, p. 1486,* doi:10.1002/mrm.26062. *Copyright (2015), © John Wiley and Sons, Inc.*

Author Manuscript Author Manuscript Author Manuscript Author Manuscript

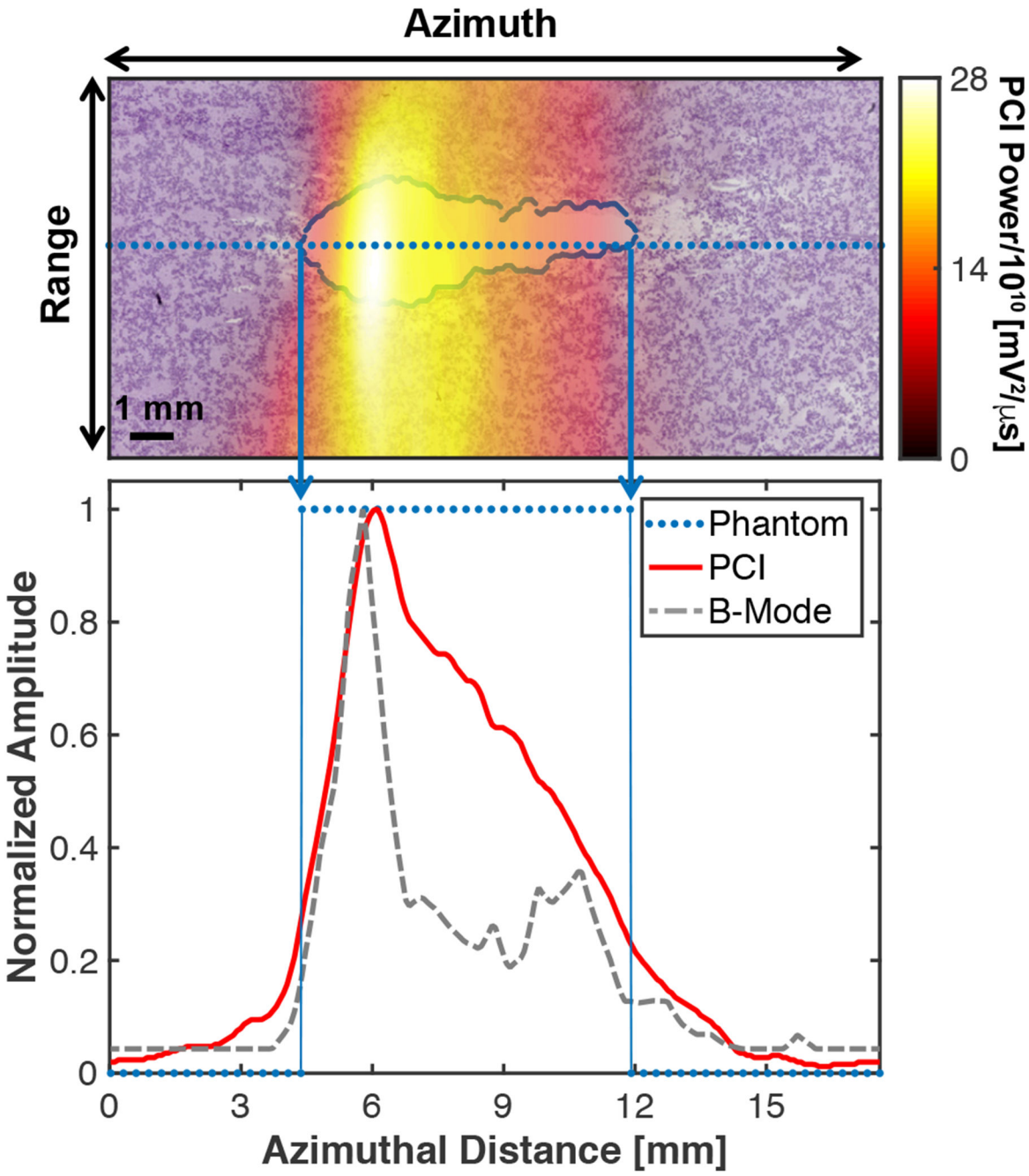

Fig. 15:

(Top panel) Passive cavitation image (PCI) registered with processed phantom image. The liquefaction zone border is outlined in blue. (Bottom panel) Comparison of the PCI and plane wave B-mode image along the dotted line in the top panel and binary phantom image. For the phantom, values of 1 indicate liquefaction, and values of 0 indicate intact phantom. The histotripsy pulse (1-MHz center frequency, 10-μs pulse duration, 18 MPa peak negative pressure) was propagating from left to right in the image (Bader et al. 2018).

Reprinted with permission from IEEE Transactions on Medical Imaging, vol. 37, Bader et al, Post hoc analysis of passive cavitation imaging for classification of histotripsy-induced liquefaction in vitro, p. 408, doi: 10.1109/TMI.2017.2735238. *Copyright (2018), © IEEE.*

Author Manuscript Author Manuscript Author Manuscript Author Manuscript